DE GRUYTER

Chemical Product and Process Modeling

Liquid- liquid flow pattern and mass transfer in a rotating millimeter channel reactor

Journal:	*Chemical Product and Process Modeling*
Manuscript ID	DGCPPM.2023.0049.R1
Manuscript Type:	Research Article
Classifications:	Process Intensification, Multi-phase flow, High-gravity technology
Keywords:	Rotating millimeter channel reactor, Liquid- liquid heterogeneous, Flow pattern, Mass transfer

SCHOLARONE™
Manuscripts

Liquid-liquid flow pattern and mass transfer in a rotating millimeter channel reactor

Liang Zheng [a,b], Yu-Hui Qi [a,b], Hai-Long Liao [a,b],

Hai-Kui Zou [a,b], Yi Ouyang[c]*, Yong Luo [a,b]*, Jian-Feng Chen [a,b]

[a]*State Key Laboratory of Organic-Inorganic Composites and* [b]*Research Center of the Ministry of Education for High Gravity Engineering and Technology, Beijing University of Chemical Technology, Beijing 100029, PR China*

[c]*Laboratory for Chemical Technology, Ghent University, Technologiepark 125, 9052 Gent, Belgium.*

* Corresponding author. Tel: +86 10 64446466; Fax: +86 10 64434784.

E-mail address: luoyong@mail.buct.edu.cn; yi.ouyang@ugent.be

For Review Only

Abstract

Currently, microchannels are widely used in liquid- liquid heterogeneous mass transfer systems due to its excellent mass transfer performance. However, because of the passive mixing principle of traditional microchannels, the improvement of mass transfer performance has a bottleneck. This work proposes a novel rotating millimeter channel reactor (RMCR), capable of achieving liquid-liquid heterogeneous mass transfer enhance by centrifugal force. Three typical flow patterns of slug flow, parallel-droplet flow, and parallel flow in the RMCR were observed by high-speed photography technology. The volumetric mass transfer coefficient ($K_O a$) of the RMCR increased with the increase of the total volumetric flow rate and rotational speed (N) increased. Compared with N = 0 r/min, the $K_O a$ of the RMCR increases by 61.5% at 200 r/min, ranging from 0.013 to 0.021 s^{-1}. The RMCR proposed in this work is expected to be applied to the liquid- liquid heterogeneous mass transfer system with high processing capacity and easy plugging.

Keywords: Rotating millimeter channel reactor; Liquid- liquid heterogeneous; Flow pattern; Mass transfer

For Review Only

1 Introduction

In recent years, microchannels have gained considerable attention due to their small size and high mass transfer efficiency (1, 2). Their unique structural characteristics have led to applications in various fields, such as chemical production, bioengineering, pharmaceuticals, environmental detection, and laboratory analysis (3-6). As a result, the implementation of microchannels in liquid-liquid mass transfer processes has emerged as a research hotspot (7-9).

Previous studies have extensively explored the structure and mass transfer properties of fixed microchannels, including T-junctions, Y-junctions, and others (10, 11). Researchers have primarily focused on geometric structure, internal mass transfer, flow patterns, and process parameter optimization in these microchannels (12). Xu et al. (13) developed two multiphase flow microfluidic devices utilizing droplet flow to enhance mass transfer performance, which shows that the droplet formation stage contributed to at least 30% of the total mass transfer. Hossain et al. examined cross-shaped microchannel reactors within Re = 0.2~ 120, revealing a mixing efficiency of up to 95% under all experimental conditions (14). Shao et al. investigated liquid-liquid microflows within a coaxial microfluidic device, observing that tiny aqueous droplets formed inside the organic phase due to mass transfer (15). Singh et al. (16) studied the hydrodynamics of liquid-liquid two-phase flow distribution in a bifurcation-based parallel microchannel, examining mass transfer performance and the formation mechanism of slug flow. These traditional fixed microchannels rely on passive mixing,

For Review Only

wherein the internal fluid flow is modified by changing the microchannel structure.

Recently, rotating microchannels employing active mixing have emerged as a research focus due to their superior mass transfer performance. Cao et al. (17) investigated the mass transfer characteristics of two immiscible fluids in a rotating spiral microchannel, where high dispersion resulted from the centrifugal force intensification. The results demonstrated that velocity and rotational speed significantly impacted extraction efficiency and average residence time. Fan et al. (18) enhanced demulsification and separation processes by developing an improved rotating microchannel (IRM) separator, finding that an appropriate increase in microchannel diameter maintained good demulsification efficiency while significantly improving organic phase separation from the upper outlet. Gandharv et al. (19) examined the effects of channel rotation, electro-osmosis, and polyelectrolyte layers on oscillatory transient behavior of flow velocities, determining that the size of the polyelectrolyte layer grafted to the walls facilitated better flow control and oscillation. Differing from rotating microchannels, Bai et al. (20) proposed a rotating millimeter channel reactor (RMCR), aiming to increase the handling capacity and performance. The RMCR can employ both centrifugal and Coriolis forces for further intensification, achieving a homogeneous micromixing efficiency 35% higher than conventional millimeter channel reactors without rotation. This combination of capillary millimeter channels and structure rotation serves as a crucial foundation for our research. Nonetheless, there remains a significant research gap in utilizing the centrifugal force generated by whole

For Review Only

structure rotation to enhance liquid-liquid heterogeneous mass transfer performance in RMCRs.

In this work, we propose a novel RMCR designed for liquid-liquid heterogeneous mass transfer. The mass transfer performance of the RMCR in a centrifugal force field was studied using a liquid-liquid system with water-kerosene. Factors influencing mass transfer performance, such as rotational speed (N), phase fraction (α), and total volumetric flow (Q_{total}), were evaluated. Our research aims to bridge the gap in understanding the potential of centrifugal force generated by whole structure rotation to improve liquid-liquid heterogeneous mass transfer performance in RMCRs, ultimately contributing to the development of more efficient and effective micro or millimeter channel technologies.

2 Experiment

2.1 Experimental Procedure

The experimental setup, illustrated in Figure 1(a), primarily consists of a high-speed camera, LED light, pump, motor, RMCR, sampling apparatus, and rotating platform. The image acquisition system was composed of a high-speed camera (Photron FASTCAM SA-Z, Photron Limited, Japan) with a lens (AF 105 mm f/8, Nikon Co., Japan) and a computer. LED lights are situated beneath the RMCR to provide ample lighting. The pump, comprising a stepper motor, control panel, and needle barrel, ensures precise flow control. The mixed fluid enters the sampling apparatus, where it

For Review Only

quickly stratifies. The phase interface area inside the sampling apparatus is minimal, making mass transfer negligible. A rotating platform, constructed from organic glass, is directly connected to the motor and serves to secure the rotating equipment. As shown in Figure 1(b), the RMCR is made of glass with a light transmittance greater than 85% to facilitate clear high-speed photography. The RMCR features a uniform thickness, an outer diameter of 4 mm, an inner diameter of 2 mm, and a length of 150 mm.

The experimental procedure can be described as follows: First, the 100ml syringe was full filled with deionized water and kerosene and installed on the pump. The RMCR is then fixed above the LED light to ensure clear visualization. Next, the inlet of the RMCR is connected to the outlet of the pump using a polyvinyl chloride hose. The high-speed camera is installed directly above the RMCR using a camera holder, connected to the computer, and adjusted for position and focus based on real-time imaging to guarantee clear visualization. According to the experimental requirements, the advancing speeds of the water and kerosene pumps are set accordingly. The motor rotational speed is also adjusted to meet the experimental needs. The pump is then turned on to expel any gas in the pipeline to prevent its influence on fluid flow. Both the pump and motor are switched on, and a 20-second waiting period allows to ensure the development of a steady flow. Finally, the high-speed camera is activated and recording begins when a stable and clear flow pattern is observed in the camera view. All experiments were conducted at 20℃.

2.2 Mass Transfer System

For Peer Review Only

Deionized water was used as the water phase, and a kerosene solution of benzoic acid served as the organic phase in the liquid-liquid mass transfer system. The concentration of benzoic acid in the kerosene was low enough to prevent changes in physicochemical properties. Table 1 displays the physical properties of the water phase and kerosene phase in the experimental system. The viscosity was measured using a viscometer (LICHEN NDJ-9S), and the interfacial tension was determined using a contact angle meter (KRÜSS DSA100).

The content of benzoic acid in water phase was measured by gas chromatography (SHIMADZU GC-2014C). The standard curve of gas chromatography was showed in Figure S1. The correlation formula fitted in the Figure S1 was used to determine the concentration of benzoic acid of the sample.

2.3 Quantification methods

When the solute is transferred from the kerosene phase to the water phase, the concentration in the kerosene phase associated with the RMCR volume (V_{RMCR}) can be expressed:

$$-Q_{\mathrm{org}} \cdot dC_{\mathrm{org}} = N_{\mathrm{O}} \cdot a \cdot dV_{\mathrm{RMCR}} \tag{2}$$

where Q_{org} is the volumetric flow of kerosene phase. C_{org} is the benzoic acid concentration in kerosene. N_{O} is the mass transfer mole flux of benzoic acid. a is the specific surface area.

Differentiating the volume of RMCR gives:

$$dV_{\mathrm{RMCR}} = \pi r^2 dL \tag{3}$$

For Review Only

where r is the inner radius of RMCR, L is the length of RMCR.

In this work, N_O is the mass transfer mole flux of benzoic acid. This could also be expressed by average driving force in kerosene phase $\left(C_{org} - C_{org}^{*}\right)$.

$$N_O = K_O\left(C_{org} - C_{org}^{*}\right) \tag{4}$$

$$C_{org}^{*} = m \cdot C_{aq} = m_0 C_{aq}^{\ 2} = 175.2 C_{aq}^{\ 2} \tag{5}$$

where K_O is overall mass transfer coefficient, m is the partition coefficient of the solute between the kerosene and water phase, which is a key parameter to characterize the mass transfer performance. This formula has been obtained in the study of Li et al. (21) as show in eq (4), where C_{aq} is the concentration of benzoic acid in the water phase, C_{org}^{*} concentration of benzoic acid in the kerosene phase at equilibrium.

In this study, the initial solute is only present in the kerosene phase, the following relation can be obtained as:

$$C_{org,\,i} = \frac{1}{D} C_{aq} + C_{org} \tag{6}$$

$$D = Q_{org} / Q_{aq} \tag{7}$$

By combing Eq (1)~ Eq (6), we get the following formula:

$$-Q_{org} \cdot \int_{C_{org,i}}^{C_{org,o}} \frac{dC_{org}}{m_0 D^2 C_{org}^{\ 2} - \left(2 m_0 C_{org,i} D^2 + 1\right) C_{org} + m_0 D^2 C_{org,i}^{\ 2}} = K_O a \cdot \pi r^2 \int_0^L dL \tag{8}$$

Discriminant of the bivariate equation in the denominator of Eq (7) is always larger than zero. And finally, the final expression of volume mass transfer coefficient $K_O a$ is obtained as:

For Review Only

$$K_{\mathrm{O}}a=\frac{Q_{\mathrm{org}}\ln\left\{\left|\frac{\left[2m_0D^2\left(c_{\mathrm{org,o}}-c_{\mathrm{org,i}}\right)-1-\sqrt{4m_0c_{\mathrm{org,i}}D^2+1}\right]\left(-1+\sqrt{4m_0c_{\mathrm{org,i}}D^2+1}\right)}{\left[2m_0D^2\left(c_{\mathrm{org,o}}-c_{\mathrm{org,i}}\right)-1+\sqrt{4m_0c_{\mathrm{org,i}}D^2+1}\right]\left(-1-\sqrt{4m_0c_{\mathrm{org,i}}D^2+1}\right)}\right|\right\}}{\pi r^2L\sqrt{4m_0c_{\mathrm{org,i}}D^2+1}} \quad (9)$$

3 Result and discussion

3.1 Flow pattern

3.1.1 Typical flow pattern

Figure 2 shows three distinct typical flow patterns in the RMCR.

$$\alpha=\frac{Q_{\mathrm{aq}}}{Q_{\mathrm{aq}}+Q_{\mathrm{org}}} \quad (10)$$

Where α is the phase fraction between water and kerosene. Figure 2(a) illustrates the formation process of slug flow (22), wherein the water and kerosene phases come into contact at the RMCR intersection and proceed together, eventually separating into two distinct liquid phases due to shearing motion. It is noteworthy that in slug flow, both the water and kerosene phases come into contact with the RMCR wall surface. In the same axial direction, the inner space of RMCR is occupied by a single-phase state. Slug breakage can be considered a result of the extrusion of the kerosene and water phases into the RMCR. The slug flow remains stable due to low flow rates and weak inter-fluid shear.

Figure 2(b) shows the development of parallel-droplet flow. The water and kerosene phases flow in parallel in the channel front section before the kerosene phase breaks evenly into small droplets, which continue flowing with water as the continuous

For Review Only

phase and kerosene as the dispersed phase. The droplet fracturing behavior exhibits fluctuations, with stability increasing as the phase fraction α increases. This fracturing occurs when the shear force between the phases surpasses the interfacial tension, causing the liquid at the kerosene phase front to separate (22).

Figure 2(c) demonstrates parallel flow (21). Following stable development, parallel flow maintains a form where water and kerosene phases exist in parallel within the channel, with no fluctuations at the phase interface. This flow pattern is prevalent when the total volumetric flow increases to a certain extent. In parallel flow, inertia force greatly exceeds interfacial tension, allowing the two-phase fluids to remain stable without fracturing. By increasing the total volumetric flow under any conditions, a stable parallel flow can ultimately be achieved.

Furthermore, carbon dust was used as a flow tracer to observe the internal flow of fluids and visualize the differences between the three typical flow patterns. Carbon dust was added to the kerosene at a ratio of 0.16 g per 100 g and left to stand for 5 minutes to form a stable suspension.

Figure 3 shows the internal flow of various flow patterns. Supporting Information (a-c) contains the original videos of Figure 3, which provide a better understanding of the flow. In general, the internal flow of kerosene varies under different flow patterns. In Figure 3(a), the movement track of toner in slug flow reveals that the flow speed at the center of the RMCR is notably higher than at other positions. Consequently, the carbon dust particles, initially at the tail, travel along the centerline to the kerosene

For Review Only

phase head and are pushed sideways. In Figure 3(b), a distinct velocity layer is observed in the kerosene phase during parallel flow. Within the kerosene phase, carbon dust particles near the phase interface progressively move ahead of those near the wall. As a result, the fluid velocity near the center of the tube is higher than that near the wall. In Figure 3(c), a turbulent internal spin is noticeable at the head of the kerosene phase (initial droplet) during parallel-droplet flow. As the front section of the parallel-droplet flow exhibits parallel flow, a high flow rate also occurs near the phase interface. This high-velocity zone extends to the head of the kerosene phase (initial droplet), inducing the internal spin. However, as the droplet detaches from the kerosene phase, its rotation speed gradually diminishes and eventually ceases.

Figure 4 further examines the internal spin of parallel-droplet flow. The movement of the flow can be seen in the videos provided in Supporting Information (d, e). The tracer streamline was also analyzed. Since particles and kerosene can be considered homogeneous, it can be processed using MATLAB (PIVLab 2.61) to obtain the corresponding vtk file. By importing the file result into paraview software, the flow field can be drawn. Figure 4(a) shows the spin in the head of the kerosene phase (initial droplet). The curved streamline of the initial droplet in Figure 4(a) effectively indicates that the internal fluid tends to rotate. The high-speed flow layer develops from the parallel-droplet flow front section, encircling the center within the head of the kerosene phase (initial droplet). The kinetic energy of the high-speed flow layer causes the head of the kerosene phase (initial droplet) to fully mix internally and be consumed by

For Review Only

friction between phase interfaces. Figure 4(b) shows the internal flow of the droplet in parallel-droplet flow. In contrast, the droplet streamline in Figure 4(b) is not curved, suggesting that the internal fluid is relatively static. The relative positions of carbon dust particles in the droplet remain constant over time, indicating that there is virtually no internal flow within the droplet. The droplet advances with the water phase. The similarities and differences in internal rotation between the two-phase fluids highlight the significant impact of shear force on the flow.

3.1.2 Effect of rotational speed on flow pattern

Figure 5 shows the flow patterns at various rotational speeds. When maintaining a constant total flow rate, the flow pattern transitions from slug flow to parallel-droplet flow as rotational speed increases, finally resulting in parallel flow. It becomes evident that the external centrifugal effect can indeed affect the flow pattern under identical conditions. This phenomenon could be attributed to the growing intensity of the external centrifugal force field, which causes a shift in the equilibrium among centrifugal effect, interfacial tension, and inertia force. As a result, the flow pattern changes at different rotational speeds.

3.1.3 Flow pattern transition

Figure 6 shows the transition curves of liquid-liquid flow patterns for the RMCR under various operational conditions. It is evident that the distribution of the three types of liquid-liquid flow patterns exhibits similar trends in different comparisons. The blue line signifies the boundary between slug flow and parallel-droplet flow, while the red

line demarcates the boundary between parallel-droplet flow and parallel flow. Slug flow primarily occurs in low total volumetric flow conditions and is less affected by rotational speed. As α increases, the sensitivity of the blue line to rotational speed progressively decreases. Parallel-droplet flow predominantly exists at medium total volumetric flow and is sensitive to rotational speed. With increasing α, the sensitivity of the red line to rotational speed continues to rise and becomes more pronounced than the blue line. Ultimately, when the total volumetric flow and rotational speed increase, the flow pattern transitions into parallel flow. It is worth noting that at high total volumetric flow, low rotational speed can result in parallel flow. However, under experimental conditions, increasing the rotational speed at low volumetric flow cannot produce parallel flow. Combined with the content in section 3.1.3, it can be concluded that the total volumetric flow is the decisive factor for the flow pattern, and the external centrifugal force field can expedite the transformation process.

Figure 6 only shows the direct effect of operating conditions on the flow pattern. If the effects of inertial forces, viscous forces, interfacial tension, and centrifugal effect on the flow pattern are considered, the operating conditions can be redescribed in dimensionless quantities to create a flow pattern distribution map. The relationship of parameter including volumetric flow of water (Q_{aq}), volumetric flow of kerosene (Q_{org}), liquid density (ρ), liquid viscosity (μ), interfacial tension between water and kerosene (σ), RMCR diameter (d), distance between the center of rotation and RMCR (r), angular velocity (ω) can be express as:

For Review Only

$$F(Q_{aq}, Q_{org}, \rho, \mu, \omega) = 0 \quad (11)$$

Based on the dimensional analysis, dimensionless groups were obtained as:

$$Re = \frac{\rho d u}{\mu} \quad (12)$$

$$\rho = \left(\frac{\alpha}{\rho_{water}} + \frac{1-\alpha}{\rho_{kerosene}} \right)^{-1} \quad (13)$$

$$\mu = \left(\frac{\alpha}{\mu_{water}} + \frac{1-\alpha}{\mu_{kerosene}} \right)^{-1} \quad (14)$$

$$Ca = \frac{\mu u}{\sigma} \quad (15)$$

$$\beta = \frac{\omega^2 r}{g} \quad (16)$$

where Re is Reynolds number, ρ is the mixing density, μ is the mixing viscosity, Ca is the Capillary number, β is the High gravity factor. The transition criterion from slug flow to parallel-droplet flow can be expressed as:

$$Ca^{-0.080}\alpha^{-0.087} = 2.39 Re^{-0.078}\beta^{0.002} \quad R^2 = 0.99 \quad (17)$$

The range of the parameters in Eq (16) are as follow: $53.01 < Re < 371.06$, $1.77 \times 10^{-3} < Ca < 1.24 \times 10^{-1}$, $0 < \beta < 4.47$ and α = 0.5/0.75/0.8. Figure 7 illustrates the corresponding transition lines. Figure 7(a) shows that the area below the transition curve indicates the formation of the parallel-droplet flow and the area above the transition curve indicates the formation of the slug flow.

The transition criterion from parallel-droplet flow to parallel flow can be expressed as:

$$Ca^{-0.087}\alpha^{-0.094} = 2.55 Re^{-0.083}\beta^{0.014} \quad R^2 = 0.98 \quad (18)$$

For Review Only

The range of the parameters in Eq (17) are as follow: $53.01 < Re < 371.06$, $1.77\times10^{-3} < Ca < 1.24\times10^{-1}$, $0 < \beta < 4.47$ and $\alpha = 0.5/0.75/0.8$. Figure 7(b) illustrates the corresponding transition lines. Figure 7(b) shows that the area below the transition curve indicates the formation of the parallel flow and the area above the transition curve indicates the formation of the parallel-droplet flow.

Combined with the results presented by the operating conditions and dimensionless quantity, it is not difficult to find that Q_{total} and N have significant influence on the flow patterns in RMCR under liquid-liquid system. Furthermore, α, Re and β play a decisive role in the flow pattern.

3.2 Mass transfer

3.2.1 Effect of flow pattern on mass transfer performance

Figure 8 shows flow patterns and K_Oa under different conditions when $\alpha = 0.5$. The different flow patterns are distinguished by its color, and the influence of different flow patterns on the K_Oa can be seen. It can be seen that in Figure 8, for a given volumetric flow, an increase in rotational speed also results in an increase in K_Oa. The range of rotational speed covered in the experiment aligns with the range of rotational speed influencing flow patterns discussed in part 3.1.3. Moreover, the K_Oa increases with the increase of total volumetric flow. It becomes evident that the addition of rotational speed and the change of total volumetric flow can change the mass transfer performance of RMCR. Taking into account the two main operating conditions-rotational speed and total volumetric flow-it can be generally stated that the K_Oa of the

For Review Only

parallel flow is higher than $K_O a$ of parallel-droplet flow than $K_O a$ of slug flow. Reason of the difference in $K_O a$ may lie in the influence of flow pattern. According to the influence of rotational speed on the mass transfer performance and the flow pattern, it is speculated that the external centrifugal force field changes the flow pattern, and then changes its mass transfer characteristics.

3.2.2 Correlation of mass transfer coefficient

The empirical formula of $K_O a$ is further fitted as follow:

$$K_O a = 0.01 Re^{0.02} Ca^{0.05} \beta^{0.15} \left(\frac{u}{L}\right) \quad R^2 = 0.96 \tag{19}$$

Thus, we can use dimensionless quantity to predict $K_O a$. The range of the parameters in eq (17) are as follow: 0.067 mL/s < Q_{aq} < 0.470 mL/s, 0.067 mL/s < Q_{org} < 0.470 mL/s and 0 < β < 4.47. It can be observed that *Re*, representing the ratio of inertial force to viscous force, has relatively large exponents, resulting in a positive effect on $K_O a$, consistent with experimental data. *Ca*, expressing the ratio of viscous force to interfacial tension, also exerts a positive influence on mass transfer. Similarly, β, the ratio of centrifugal force to inertial force, positively affects mass transfer. This suggests that the external centrifugal force field indeed enhances the liquid-liquid heterogeneous mass transfer performance of the RMCR. The fitted correlation predicts all $K_O a$ values to be within ± 20% of the experimental data, as demonstrated in Figure 9.

4 Conclusions

For Review Only

In this study, a novel RMCR was proposed, and its liquid-liquid heterogeneous mass transfer performance was investigated in the water-benzoic acid-kerosene system using high-speed photography. Employing high-speed photography technology, we identified three typical flow patterns in the RMCR: slug flow, parallel-droplet flow, and parallel flow. Dimensionless fitting allows to determine the flow pattern transition criteria from slug flow to parallel-droplet flow and from parallel-droplet flow to parallel flow. Additionally, it is found that the total flow rate and rotational speed are the primary parameters governing the flow pattern. As the rotational speed and total flow rate increase, the $K_O a$ of the RMCR continues to rise, ranging from 0.003 to 0.021 s^{-1}. A correlation for predicting the mass transfer coefficient was proposed, and the predicted values showed good agreement with experimental values, with deviations within ±20%.

Acknowledgment

This work was supported by the National Natural Science Foundation of China (Nos. 22288102 and 22378011).

Supplementary materials

Figure S1. Standard curve of gas chromatography.

Supplementary data associated with this article can be found in the online version.

a. Behavior of the tracer in the slug flow - Figure 3(a) - 10 times speed down

b. Behavior of the tracer in the parallel-droplet flow - Figure 3(b) - 10 times speed

For Review Only

down

c. Behavior of the tracer in the parallel flow - Figure 3(c) - 100 times speed down

d. Behavior of the tracer in the parallel-droplet flow (initial droplet) - Figure 4(a) - 30 times speed down

e. Behavior of the tracer in the parallel-droplet flow (final droplet) - Figure 4(b) - 30 times speed down

For Review Only

Nomenclature

Q_{total}	total volumetric flow rate	mL/s
N	RMCR rotation speed	r/min
d	inner diameter of the RMCR	m
N_O	mole flux of benzoic acid	mol/(m^2·s^1)
D	ratio of kerosene phase to water phase	-
V_{RMCR}	The volume of the RMCR	m^3
a	specific surface area	m^2/m^3
K_O	overall mass transfer coefficient	m/s
$C_{aq,i}$	concentration of benzoic acid in the water phase at the inlet	mol/m^3
$C_{aq,o}$	concentration of benzoic acid in the water phase at the outlet	mol/m^3
$C_{org,i}$	concentration of benzoic acid in the kerosene phase at the inlet	mol/m^3
$C_{org,o}$	concentration of benzoic acid in the kerosene phase at the outlet	mol/m^3
C^*_{org}	concentration of benzoic acid in the kerosene phase at equilibrium	mol/m^3
V_{RMCR}	volume within the RMCR	m^3
L	length of the RMCR	m
r	The radius of rotation of RMCR	m

Greek Letters

ρ	density	kg/m^3
μ	viscosity	mPa·s
σ	interfacial tension between water and kerosene	mN/m
ω	RMCR angular velocity	rad/s
β	high gravity factor	-

For Review Only

α	phase fraction between water and kerosene	-

Dimensionless group

Re	Reynolds number
Ca	Capillary number

Abbreviations

RMCR	Rotating millimeter channel reactor
MCR	Millimeter channel reactor

For Review Only

References

1.Wang K, Luo GS. Microflow extraction: A review of recent development. Chemical Engineering Science. 2017;169:18-33.

2.Mills PL, Quiram DJ, Ryley JF. Microreactor technology and process miniaturization for catalytic reactions - A perspective on recent developments and emerging technologies. Chemical Engineering Science. 2007;62(24):6992-7010.

3.Doku GN, Verboom W, Reinhoudt DN, van den Berg A. On-microchip multiphase chemistry - A review of microreactor design principles and reagent contacting modes. Tetrahedron. 2005;61(11):2733-2742.

4.Mae K. Advanced chemical processing using microspace. Chemical Engineering Science. 2007;62(18-20):4842-4851.

5.Assmann N, Ładosz A, Rudolf von Rohr P. Continuous Micro Liquid-Liquid Extraction. Chemical Engineering & Technology. 2013;36(6):921-936.

6.Porta R, Benaglia M, Puglisi A. Flow Chemistry: Recent Developments in the Synthesis of Pharmaceutical Products. Organic Process Research & Development. 2015;20(1):2-25.

7.Sattari-Najafabadi M, Nasr Esfahany M, Wu Z, Sunden B. Mass transfer between phases in microchannels: A review. Chemical Engineering and Processing - Process Intensification. 2018;127:213-237.

8.Yao CQ, Zhao YC, Chen GW. Multiphase processes with ionic liquids in microreactors: hydrodynamics, mass transfer and applications. Chemical Engineering

For Review Only

Science. 2018;189:340-359.

9.Angeli P, Tsaoulidis D, Hashi Weheliye W. Studies on mass transfer of europium(III) in micro-channels using a micro Laser Induced Fluorescence technique. Chemical Engineering Journal. 2019;372:1154-1163.

10.Tan J, Xu JH, Li SW, Luo GS. Drop dispenser in a cross-junction microfluidic device: Scaling and mechanism of break-up. Chemical Engineering Journal. 2008;136(2-3):306-311.

11.Roques-Carmes T, Monnier H, Portha JF, Marchal P, Falk L. Influence of the plate-type continuous micro-separator dimensions on the efficiency of demulsification of oil-in-water emulsion. Chemical Engineering Research and Design. 2014;92(11):2758-69.

12.Kolehmainen E, Turunen I. Micro-scale liquid-liquid separation in a plate-type coalescer. Chemical Engineering and Processing: Process Intensification. 2007;46(9):834-839.

13.Xu JH, Tan J, Li SW, Luo GS. Enhancement of mass transfer performance of liquid-liquid system by droplet flow in microchannels. Chemical Engineering Journal. 2008;141(1-3):242-249.

14.Hossain S, Lee I, Kim SM, Kim KY. A micromixer with two-layer serpentine crossing channels having excellent mixing performance at low Reynolds numbers. Chemical Engineering Journal. 2017;327:268-277.

15.Shao H, LÜ Y, Wang K, Luo GS. An Experimental Study of Liquid-Liquid Microflow Pattern Maps Accompanied with Mass Transfer. Chinese Journal of

For Review Only

Chemical Engineering. 2012;20(1):18-26.

16.Singh S, Kumar UKA. Hydrodynamics and Mass Transfer Studies of Liquid-Liquid Two-Phase Flow in Parallel Microchannels. International Journal of Multiphase Flow. 2022;157:104248.

17.Cao Y, Li J, Jin Y, Luo JH, Wang YB. Liquid-liquid two-phase mass transfer characteristics in a rotating helical microchannel. Chinese Journal of Chemical Engineering. 2019;27(12):2937-2947.

18.Fan CX, Guo ZN, Luo JH. Study on an improved rotating microchannel separator in the intensification for demulsification and separation process. Chinese Journal of Chemical Engineering. 2022;55:181-191.

19.Gandharv S, Kaushik P. Transient electro-osmotic flow in rotating soft microchannel. Physics of Fluids. 2022;34(8):082023.

20.Bai S, Li WS, Liu W, Luo Y, Chu GW, Chen JF. Micromixing efficiency intensification of a millimeter channel reactor in the high gravity field. Chemical Engineering Science. 2022;251:117407.

21.Li WP, Xia FS, Zhao SC, Zhang MQ, Li W, Zhang JL. Characterization of liquid-liquid mass transfer performance in a novel pore‐array intensified tube‐in‐tube microchannel. AIChE Journal. 2019;66(4).

22 Shin, H.C.; Kim, S.M. Experimental investigation of two-phase flow regimes in rectangular micro-channel with two mixer types. Chemical Engineering Journal 2022, 448:137581.

For Review Only

418

419

For Review Only

Figure Captions

Figure 1. Schematic diagram of (a) experimental setup and (b) RMCR.

Figure 2. Typical dynamic process of (a) image acquisition window, (b) slug flow when Q_{total} = 0.134 mL/s and α = 0.5, (c) parallel-droplet flow when Q_{total} = 0.281 mL/s and α = 0.8, (d) parallel flow when Q_{total} = 1.54 mL/s and α = 0.5.

Figure 3. Behavior of the tracer in the (a) slug flow, (b) parallel-droplet flow, (c) parallel flow.

Figure 4. Streamline of internal rotation flow of parallel-droplet flow in different stages (a) initial droplet, (b) droplet.

Figure 5. Effect of rotational speed on flow pattern when (a) Q_{total} = 0.267 mL/s and α = 0.5, (b) Q_{total} = 0.134 mL/s and α = 0.75, (c) Q_{total} = 0.134 mL/s and α = 0.8.

Figure 6. Liquid flow pattern transition curves for (a) α = 0.5, (b) α = 0.75, (c) α = 0.8.

Figure 7. Liquid flow transition criteria from (a) slug flow to parallel-droplet flow, (b) parallel-droplet flow to parallel flow.

Figure 8. Flow patterns and $K_O a$ under different operating conditions.

Figure 9. Comparison of predicted and experimental values of $K_O a$.

Table Legend

Table 1. Physical properties of mass transfer system (20 ℃).

For Review Only

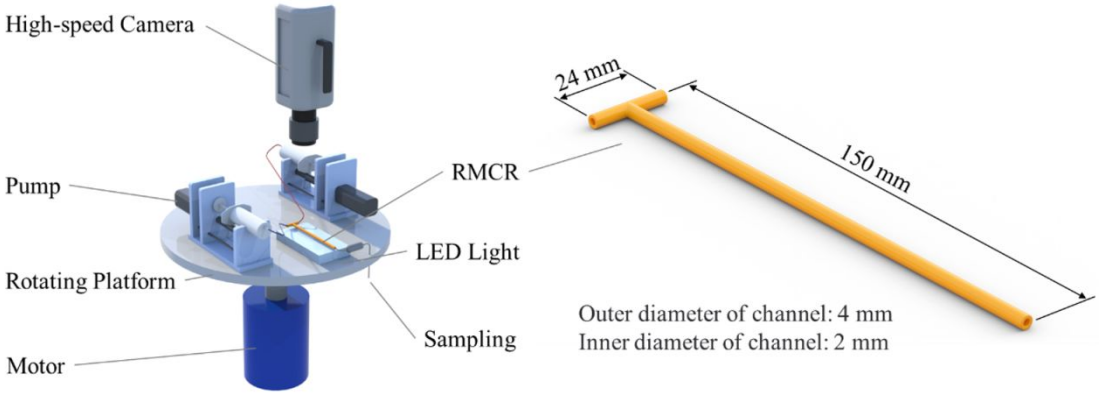

(a) (b)

Figure 1. Schematic diagram of (a) experimental setup and (b) RMCR.

For Review Only

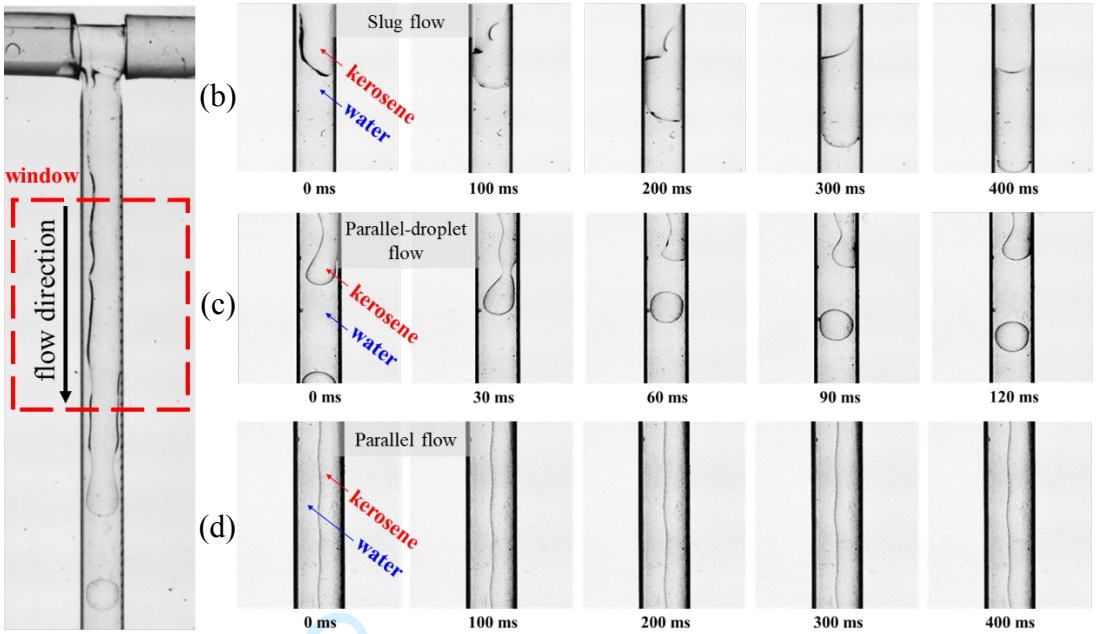

Figure 2. Typical dynamic process of (a) image acquisition window, (b) slug flow when Q_{total} = 0.134 mL/s and α = 0.5, (c) parallel-droplet flow when Q_{total} = 0.281 mL/s and α = 0.8, (d) parallel flow when Q_{total} = 1.54 mL/s and α = 0.5.

For Review Only

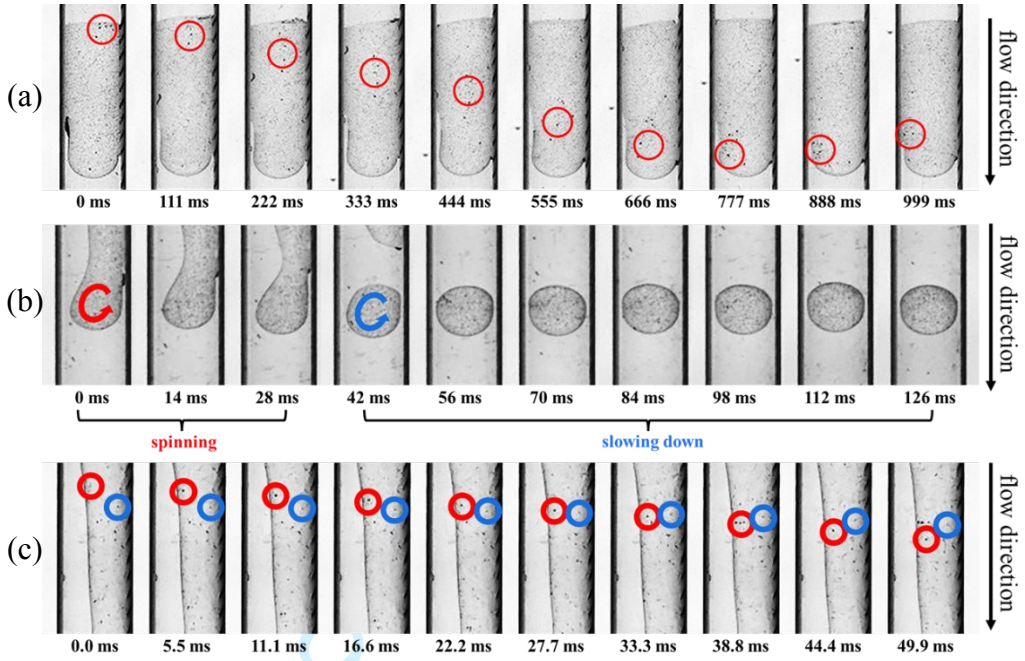

Figure 3. Behavior of the tracer in the (a) slug flow, (b) parallel-droplet flow, (c) parallel flow.

For Review Only

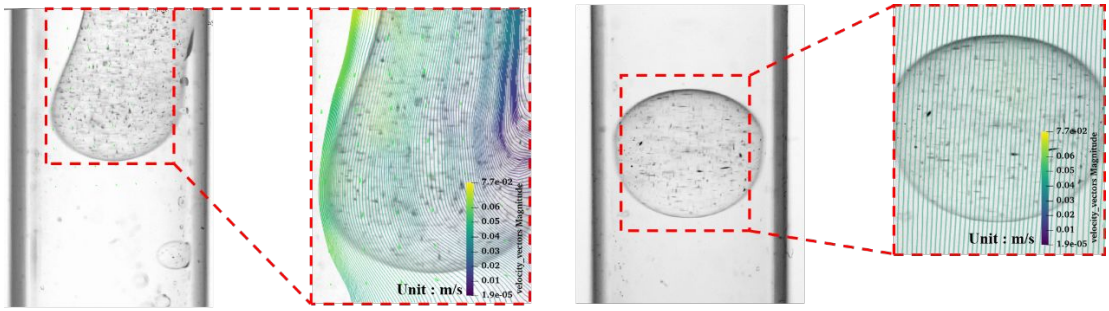

(a) (b)

Figure 4. Streamline of internal rotation flow of parallel-droplet flow in different stages (a) initial droplet, (b) droplet.

For Review Only

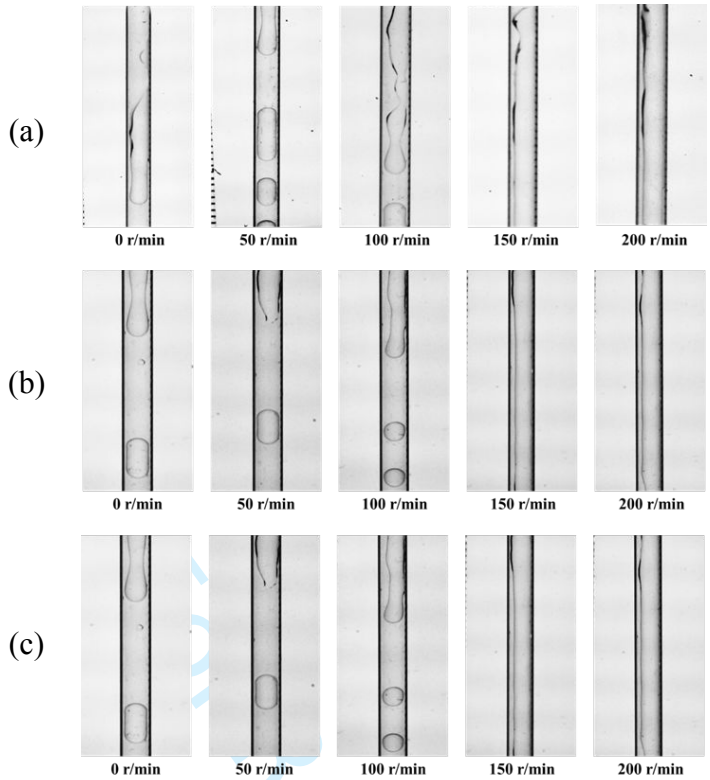

Figure 5. Effect of rotational speed on flow pattern when (a) Q_{total} = 0.267 mL/s and α = 0.5, (b) Q_{total} = 0.134 mL/s and α = 0.75, (c) Q_{total} = 0.134 mL/s and α = 0.8.

For Review Only

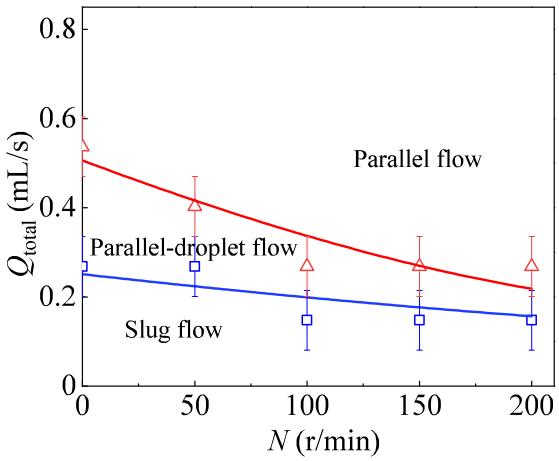

(a)

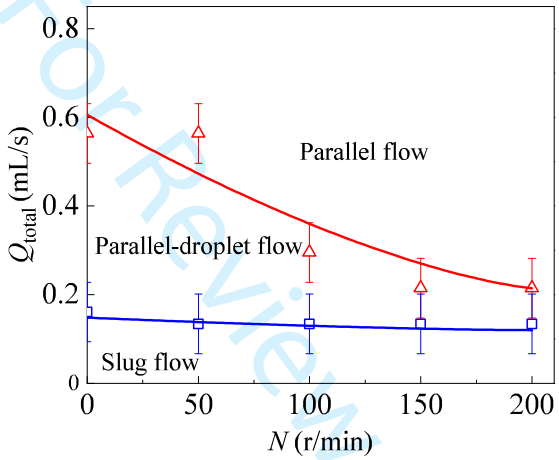

(b)

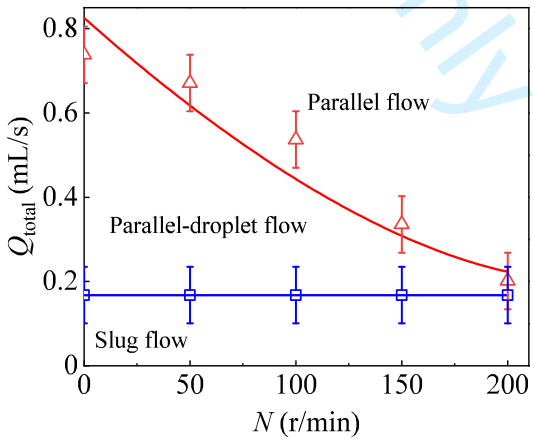

(c)

Figure 6. Liquid flow pattern transition curves for (a) $\alpha = 0.5$, (b) $\alpha = 0.75$, (c) $\alpha = 0.8$.

For Review Only

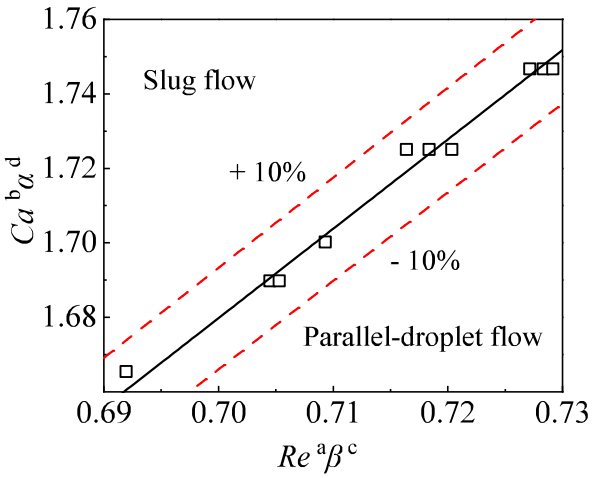

(a)

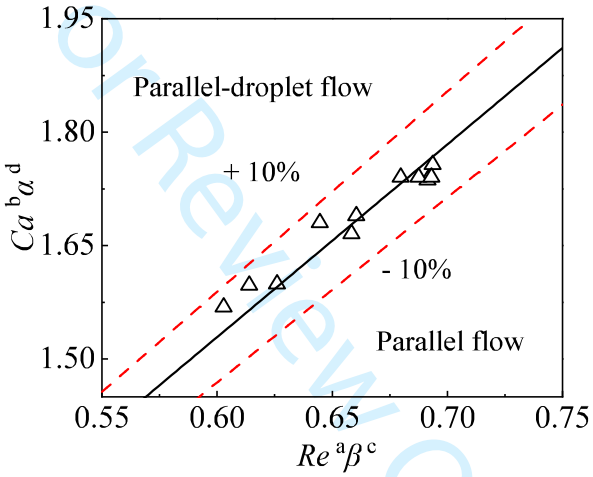

(b)

Figure 7. Liquid flow transition criteria from (a) slug flow to parallel-droplet flow, (b) parallel-droplet flow to parallel flow.

For Review Only

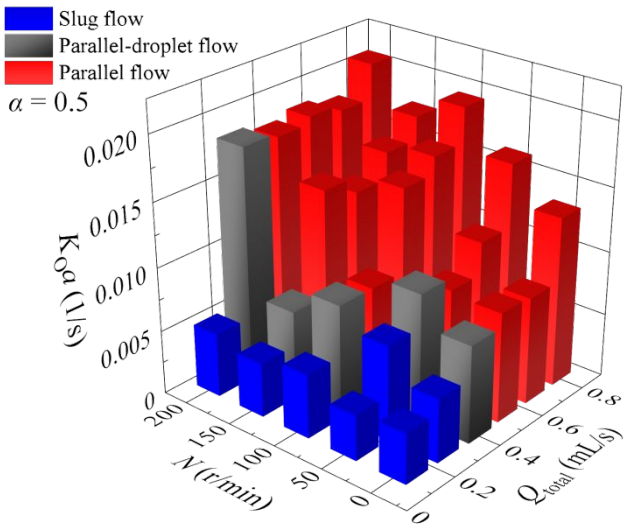

Figure 8. Flow patterns and K_Oa under different operating conditions.

For Review Only

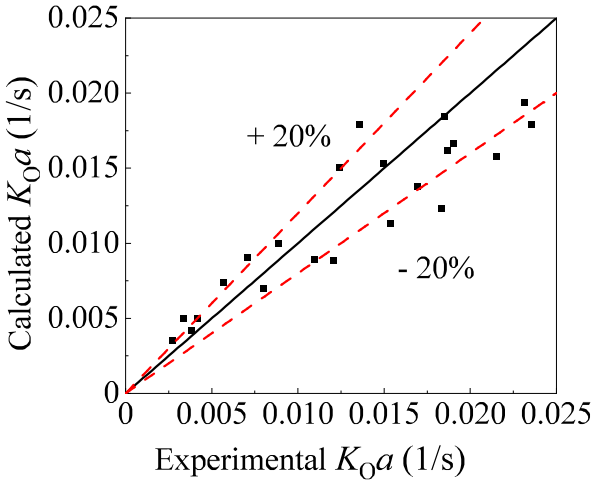

Figure 9. Comparison between predicted and experimental values of $K_O a$.

For Review Only

Table 1. Physical properties of mass transfer system (20 ℃)

Phase	Solvend	ρ / kg·m^{-3}	μ / mPa·s	σ / mN·m^{-1}
Water	-	998.182	1.005	34.574
Kerosene	benzoic acid (0.2w%)	799.096	2.500	

For Review Only

Reply to the comments from Reviewers:

Reviewer #1:

√ We thank the reviewer for the comments to improve the quality of this manuscript. We have responded to all the comments point by point. The revised contents have been marked as yellow color in the revised manuscript.

The paper is not clear in the experimental explanation.
a- The setup and the methodology of running the experiments is the main section and must be developed with details. For example, the high speed camera and lighting are the heart of these experiments that need more explanations.
√ Thanks for your suggestions. The experimental procedure can be described as follows. First, fill a 100 mL syringe with deionized water and kerosene and then installed on the pump. The RMCR is then fixed above the LED light to ensure clear visualization. Next, the inlet of the RMCR is connected to the outlet of the pump using a polyvinyl chloride hose. The high-speed camera is installed directly above the RMCR using a camera holder, connected to the computer, and adjusted for position and focus based on real-time imaging to guarantee clear visualization. According to the experimental requirements, the feeding speeds of the water and kerosene pumps are set accordingly. The motor rotational speed is also adjusted to meet the experimental needs. The pump is then turned on to expel any gas in the pipeline to prevent its influence on fluid flow. Both the pump and motor are switched on, and a 20 s waiting period allows to ensure the development of a steady flow. Finally, the high-speed camera is recording when a stable and clear flow pattern is observed in the camera view. All experiments were conducted at 20 ℃. The above issues have been modified in the revised manuscript in Page 6, Lines 101-114.

b- There are several vague sentences in the experimental section that must be cleared. For example, in the page7 "an appropriate amount of deionized water ...). They should mention the exact amount or explain how they calculate/measure the appropriate amount. The other researchers should be able to duplicate those experiments and these data are necessary.
√ Thans for your advice. The 100 mL syringe was full filled with deionized water. And other similar sentences also have been revised. The above issue has been modified in the revised manuscript in Page 6, Lines 101.

c- How do they capture the streamlines in graph 5? It needs more explanations, not just one sentence on page 11.
√ Thanks for your comments this point. Since particles and kerosene can be considered homogeneous, it can be processed using MATLAB (PIVLab 2.61) to obtain the corresponding vtk file. By importing the file result into paraview software, the flow field can be drawn. The above issue has been modified in the revised manuscript in Page 11, Lines 208-211.

1- The quality of images should be improved such as fig 9

For Review Only

√ Thans for your advice. Since the window required for shooting is about 10 mm, the lens magnification suitable for this shooting condition cannot be changed. We have processed the raw material to the clearest possible look to ensure accuracy. The video we provided can be more clear for readers .

2- The references are not consistent, e.g., Ref- 14 & 15.

√ Thanks for your suggestions. We have made changes to the format of the references.

For Review Only

Reviewer #2:

This paper investigates the effect of centrifugal force on flow patterns and mass transfer inside the microchannel with the help of high-speed imaging. They found three flow patterns with the change of total volumetric flow rate, phase fraction between water and kerosene, and rotational speed. Results were validated against experimental data, and the study revealed the centrifugal force resulting from the rotational speed parameter, causes the flow pattern's variation. As the rotational speed and the total flow rate increase, the mass transfer inside the microchannel rises. Also, they proposed a correlation for the prediction of the mass transfer coefficient. The research could provide helpful knowledge regarding the factors influencing mass transfer within microchannels. However, the paper needs a major revision as it does not meet the standards of a journal paper.

√ We thank the reviewer for the comments to improve the quality of this manuscript. We have responded to all the comments point by point. The revised contents have been marked as yellow color in the revised manuscript.

My main comments are as follows:

The novelty of the study is not clear. Since you mentioned "it can be concluded that the total volumetric flow is the decisive factor for the flow pattern, and the external centrifugal force field can expedite the transformation process", the presence of the centrifugal effect can not help the mass transfer significantly.

√ Thanks for your comments. In this work, we found that both the total volumetric flow and the external centrifugal force field can affect mass transfer, and the total volumetric flow has the most significant effect. The innovation of this work more focused on the discovery of the effect of external centrifugal force field on the millimeter channel, because the effect of total volumetric flow has been extensively verified in previous studies. This discovery provides a new way to improve the mass transfer efficiency of channel reactor in the future.

There are numerous typos throughout the paper which should be solved. For example, Liquid-liquid in the title should not have a space before the second liquid.

√ Thanks for this point. We have corrected the wording of the title.

Authors evaluated the mass transfer coefficient of liquids inside the microchannel, while they did not consider the role of temperature in their experiments. It is important to take the temperature into account for mass transfer evaluation. Indeed, authors did not provide a condition that temperature is constant in all their experiments.

√ Thanks for this advice very much. In fact, all of our experiments were conducted at 20 ℃. We have added temperature conditions in the Experimental Procedure Section.

The start of each section is unclear. For example, in the result and discussion, there is no connection between sections and paragraphs, which makes the paper for readers ambiguous.

√ Thans for your advice. We have made corresponding modifications to the Results and

Discussion Section.

No comparison has been made between their results and the existing literature. It is crucial for authors asserting the novelty of their findings in a microchannel to conduct a comparative analysis, demonstrating the importance of their work.
√ This is a very nice comment on our research. Most studies compare their results with the references. But what is different in this paper is the form of centrifugal force intervention. The former rotating channel adopts the structure form of tube-in-tube, which is directly manifested as the shear action of fluid between two layers of wall surface. However, the fluid in this study is directly affected by the centrifugal force field, and the intensification mechanism is different. This is already mentioned in the Introduction Section.

Other comments:
The figures have low resolution and quality, and they should be significantly improved.
√ Thans for your advice. Since the window required for shooting is about 10 mm, the lens magnification suitable for this shooting condition cannot be changed. We have processed the raw material to the clearest possible look to ensure accuracy. The video we provided can be more clear for readers.

In several parts, the paper claims some information without any proof or references!
√ Thans for your advice. We have made corresponding modifications to the full text and checked the part of references.

Centrifugal force is not a good phrase since you do not measure the force. Indeed, it is better to use the centrifugal effect.
√ Thans for your advice. We have revised the presentation in the text to make it more appropriate. It has been modified in the revised manuscript in Pages 12, Lines 227-231, Pages 13, Lines 252-254.

Table 1 is not useful and the details of the camera can be shared in one sentence.
√ Thanks for this point. The image acquisition system was composed of a high-speed camera (Photron FASTCAM SA-Z, Photron Limited, Japan) with a lens (AF 105 mm f/8, Nikon Co., Japan) and a computer. It has been modified in the revised manuscript in Pages 5, Lines 90-92.

Also, Figure 2 does not add any point to the paper. It can be brought in supplementary material.
√ Thanks for this point. We have deleted Figure 2 in the manuscript and added it to Supplementary Material. The above issue has been modified in the revised Supplementary Material in Pages 2.

In (3.1.1 Typical flow pattern), I do not understand the change of which parameter leads to the variation of flow patterns. Please explain it in more detail.
√ Thanks for this point. Part 3.1.1 is used only to illustrate typical flow patterns. The

For Review Only

factors affecting the flow pattern are explained in detail in Section "3.1.3 Flow pattern transition", and the flow pattern distribution diagram is provided for reference.

Please bring some related references to (3.1.1 Typical flow pattern). I provided two references as follows: (https://doi.org/10.1016/j.jtice.2022.104602) and (https://doi.org/10.1016/j.ces.2008.05.005)
√ Thanks for this point. We have modified the expression here and cited the above two papers. It has been modified in the revised manuscript in Pages 9-10, Lines 163-185.

The phase fraction is not identified in the first part of the paper, and you used it in the results once. Please specify it first, then use it in other parts of the paper.
√ Thanks for this point. α is the phase fraction between water and kerosene. It has been modified in the revised manuscript in Pages 9, Lines 162.

The term "shear force" is employed without adequate clarification or measurement.
√ Thanks for this point. We have revised the expression here and added the references. It has been modified in the revised manuscript in Pages 10, Lines 176-178.

Please add references when you bring a fact or reason for a phenomenon. For example "This phenomenon could be attributed to the growing intensity of the external centrifugal force field, which causes a shift in the equilibrium among centrifugal force, interfacial tension, and inertia force."
√ Thanks for this point. We have optimized the citation of references.

21.Li WP, Xia FS, Zhao SC, Zhang MQ, Li W, Zhang JL. Characterization of liquid-liquid mass transfer performance in a novel pore-array intensified tube-in-tube microchannel. AIChE Journal. 2019;66(4).
22 Shin, H.C.; Kim, S.M. Experimental investigation of two-phase flow regimes in rectangular micro-channel with two mixer types. Chemical Engineering Journal 2022, 448:137581.

While β is the ratio of centrifugal force to inertial force, it cannot be concluded that it is an indicator of the centrifugal effect since it changes with the volume flow rate. Therefore, your suggestion in the following part may be incorrect: "This suggests that the external centrifugal force field indeed enhances the liquid-liquid heterogeneous mass transfer performance of the RMCR."
√ This is a very nice view on our research focus. In fact, β does not change with the volumetric flow. The expression for β is $\beta = \frac{\omega^2 r}{g}$. Volumetric flow does not participate in β's calculation.

There is not any discussion in your result and discussion section. So, it is better to

remove it

√ Thans for your advice. We have made corresponding modifications to the Results and Discussion Section. Thank you again for the important and useful comments for us to improve the quality of this manuscript.

For Review Only

Liquid-liquid flow pattern and mass transfer in a rotating millimeter channel reactor

Liang Zheng [a,b], Yu-Hui Qi [a,b], Hai-Long Liao [a,b],
Hai-Kui Zou [a,b], Yi Ouyang[c]*, Yong Luo [a,b]*, Jian-Feng Chen [a,b]

[a]*State Key Laboratory of Organic-Inorganic Composites and* [b]*Research Center of the Ministry of Education for High Gravity Engineering and Technology, Beijing University of Chemical Technology, Beijing 100029, PR China*

[c]*Laboratory for Chemical Technology, Ghent University, Technologiepark 125, 9052 Gent, Belgium.*

* Corresponding author. Tel: +86 10 64446466; Fax: +86 10 64434784.
E-mail address: luoyong@mail.buct.edu.cn; yi.ouyang@ugent.be

For Review Only

Abstract

Currently, microchannels are widely used in liquid- liquid heterogeneous mass transfer systems due to its excellent mass transfer performance. However, because of the passive mixing principle of traditional microchannels, the improvement of mass transfer performance has a bottleneck. This work proposes a novel rotating millimeter channel reactor (RMCR), capable of achieving liquid-liquid heterogeneous mass transfer enhance by centrifugal force. Three typical flow patterns of slug flow, parallel-droplet flow, and parallel flow in the RMCR were observed by high-speed photography technology. The volumetric mass transfer coefficient ($K_O a$) of the RMCR increased with the increase of the total volumetric flow rate and rotational speed (N) increased. Compared with N = 0 r/min, the $K_O a$ of the RMCR increases by 61.5% at 200 r/min, ranging from 0.013 to 0.021 s^{-1}. The RMCR proposed in this work is expected to be applied to the liquid- liquid heterogeneous mass transfer system with high processing capacity and easy plugging.

Keywords: Rotating millimeter channel reactor; Liquid- liquid heterogeneous; Flow pattern; Mass transfer

For Review Only

1 Introduction

In recent years, microchannels have gained considerable attention due to their small size and high mass transfer efficiency (1, 2). Their unique structural characteristics have led to applications in various fields, such as chemical production, bioengineering, pharmaceuticals, environmental detection, and laboratory analysis (3-6). As a result, the implementation of microchannels in liquid-liquid mass transfer processes has emerged as a research hotspot (7-9).

Previous studies have extensively explored the structure and mass transfer properties of fixed microchannels, including T-junctions, Y-junctions, and others (10, 11). Researchers have primarily focused on geometric structure, internal mass transfer, flow patterns, and process parameter optimization in these microchannels (12). Xu et al. (13) developed two multiphase flow microfluidic devices utilizing droplet flow to enhance mass transfer performance, which shows that the droplet formation stage contributed to at least 30% of the total mass transfer. Hossain et al. examined cross-shaped microchannel reactors within Re = 0.2~ 120, revealing a mixing efficiency of up to 95% under all experimental conditions (14). Shao et al. investigated liquid-liquid microflows within a coaxial microfluidic device, observing that tiny aqueous droplets formed inside the organic phase due to mass transfer (15). Singh et al. (16) studied the hydrodynamics of liquid-liquid two-phase flow distribution in a bifurcation-based parallel microchannel, examining mass transfer performance and the formation mechanism of slug flow. These traditional fixed microchannels rely on passive mixing,

For Review Only

wherein the internal fluid flow is modified by changing the microchannel structure.

Recently, rotating microchannels employing active mixing have emerged as a research focus due to their superior mass transfer performance. Cao et al. (17) investigated the mass transfer characteristics of two immiscible fluids in a rotating spiral microchannel, where high dispersion resulted from the centrifugal force intensification. The results demonstrated that velocity and rotational speed significantly impacted extraction efficiency and average residence time. Fan et al. (18) enhanced demulsification and separation processes by developing an improved rotating microchannel (IRM) separator, finding that an appropriate increase in microchannel diameter maintained good demulsification efficiency while significantly improving organic phase separation from the upper outlet. Gandharv et al. (19) examined the effects of channel rotation, electro-osmosis, and polyelectrolyte layers on oscillatory transient behavior of flow velocities, determining that the size of the polyelectrolyte layer grafted to the walls facilitated better flow control and oscillation. Differing from rotating microchannels, Bai et al. (20) proposed a rotating millimeter channel reactor (RMCR), aiming to increase the handling capacity and performance. The RMCR can employ both centrifugal and Coriolis forces for further intensification, achieving a homogeneous micromixing efficiency 35% higher than conventional millimeter channel reactors without rotation. This combination of capillary millimeter channels and structure rotation serves as a crucial foundation for our research. Nonetheless, there remains a significant research gap in utilizing the centrifugal force generated by whole

For Review Only

structure rotation to enhance liquid-liquid heterogeneous mass transfer performance in RMCRs.

In this work, we propose a novel RMCR designed for liquid-liquid heterogeneous mass transfer. The mass transfer performance of the RMCR in a centrifugal force field was studied using a liquid-liquid system with water-kerosene. Factors influencing mass transfer performance, such as rotational speed (N), phase fraction (α), and total volumetric flow (Q_{total}), were evaluated. Our research aims to bridge the gap in understanding the potential of centrifugal force generated by whole structure rotation to improve liquid-liquid heterogeneous mass transfer performance in RMCRs, ultimately contributing to the development of more efficient and effective micro or millimeter channel technologies.

2 Experiment

2.1 Experimental Procedure

The experimental setup, illustrated in Figure 1(a), primarily consists of a high-speed camera, LED light, pump, motor, RMCR, sampling apparatus, and rotating platform. The image acquisition system was composed of a high-speed camera (Photron FASTCAM SA-Z, Photron Limited, Japan) with a lens (AF 105 mm f/8, Nikon Co., Japan) and a computer. LED lights are situated beneath the RMCR to provide ample lighting. The pump, comprising a stepper motor, control panel, and needle barrel, ensures precise flow control. The mixed fluid enters the sampling apparatus, where it

For Review Only

quickly stratifies. The phase interface area inside the sampling apparatus is minimal, making mass transfer negligible. A rotating platform, constructed from organic glass, is directly connected to the motor and serves to secure the rotating equipment. As shown in Figure 1(b), the RMCR is made of glass with a light transmittance greater than 85% to facilitate clear high-speed photography. The RMCR features a uniform thickness, an outer diameter of 4 mm, an inner diameter of 2 mm, and a length of 150 mm.

The experimental procedure can be described as follows: First, the 100ml syringe was full filled with deionized water and kerosene and installed on the pump. The RMCR is then fixed above the LED light to ensure clear visualization. Next, the inlet of the RMCR is connected to the outlet of the pump using a polyvinyl chloride hose. The high-speed camera is installed directly above the RMCR using a camera holder, connected to the computer, and adjusted for position and focus based on real-time imaging to guarantee clear visualization. According to the experimental requirements, the advancing speeds of the water and kerosene pumps are set accordingly. The motor rotational speed is also adjusted to meet the experimental needs. The pump is then turned on to expel any gas in the pipeline to prevent its influence on fluid flow. Both the pump and motor are switched on, and a 20-second waiting period allows to ensure the development of a steady flow. Finally, the high-speed camera is activated and recording begins when a stable and clear flow pattern is observed in the camera view. All experiments were conducted at 20℃.

2.2 Mass Transfer System

Deionized water was used as the water phase, and a kerosene solution of benzoic acid served as the organic phase in the liquid-liquid mass transfer system. The concentration of benzoic acid in the kerosene was low enough to prevent changes in physicochemical properties. Table 1 displays the physical properties of the water phase and kerosene phase in the experimental system. The viscosity was measured using a viscometer (LICHEN NDJ-9S), and the interfacial tension was determined using a contact angle meter (KRÜSS DSA100).

The content of benzoic acid in water phase was measured by gas chromatography (SHIMADZU GC-2014C). The standard curve of gas chromatography was showed in Figure S1. The correlation formula fitted in the Figure S1 was used to determine the concentration of benzoic acid of the sample.

2.3 Quantification methods

When the solute is transferred from the kerosene phase to the water phase, the concentration in the kerosene phase associated with the RMCR volume (V_{RMCR}) can be expressed:

$$-Q_{\mathrm{org}} \cdot dC_{\mathrm{org}} = N_{\mathrm{O}} \cdot a \cdot dV_{\mathrm{RMCR}} \tag{2}$$

where Q_{org} is the volumetric flow of kerosene phase. C_{org} is the benzoic acid concentration in kerosene. N_{O} is the mass transfer mole flux of benzoic acid. a is the specific surface area.

Differentiating the volume of RMCR gives:

$$dV_{\mathrm{RMCR}} = \pi r^2 dL \tag{3}$$

For Review Only

where r is the inner radius of RMCR, L is the length of RMCR.

In this work, N_O is the mass transfer mole flux of benzoic acid. This could also be expressed by average driving force in kerosene phase $\left(C_{org} - C_{org}^{*}\right)$.

$$N_O = K_O\left(C_{org} - C_{org}^{*}\right) \tag{4}$$

$$C_{org}^{*} = m \cdot C_{aq} = m_0 C_{aq}^{\ 2} = 175.2 C_{aq}^{\ 2} \tag{5}$$

where K_O is overall mass transfer coefficient, m is the partition coefficient of the solute between the kerosene and water phase, which is a key parameter to characterize the mass transfer performance. This formula has been obtained in the study of Li et al. (21) as show in eq (4), where C_{aq} is the concentration of benzoic acid in the water phase, C_{org}^{*} concentration of benzoic acid in the kerosene phase at equilibrium.

In this study, the initial solute is only present in the kerosene phase, the following relation can be obtained as:

$$C_{org,\,i} = \frac{1}{D} C_{aq} + C_{org} \tag{6}$$

$$D = Q_{org} / Q_{aq} \tag{7}$$

By combing Eq (1)~ Eq (6), we get the following formula:

$$-Q_{org} \cdot \int_{C_{org,i}}^{C_{org,o}} \frac{dC_{org}}{m_0 D^2 C_{org}^{\ 2} - \left(2 m_0 C_{org,i} D^2 + 1\right) C_{org} + m_0 D^2 C_{org,i}^{\ 2}} = K_O a \cdot \pi r^2 \int_0^L dL \tag{8}$$

Discriminant of the bivariate equation in the denominator of Eq (7) is always larger than zero. And finally, the final expression of volume mass transfer coefficient $K_O a$ is obtained as:

For Review Only

$$K_{\mathrm{O}}a=\frac{Q_{\mathrm{org}}\ln\left\{\left|\frac{\left[2m_0D^2\left(c_{\mathrm{org,o}}-c_{\mathrm{org,i}}\right)-1-\sqrt{4m_0c_{\mathrm{org,i}}D^2+1}\right]\left(-1+\sqrt{4m_0c_{\mathrm{org,i}}D^2+1}\right)}{\left[2m_0D^2\left(c_{\mathrm{org,o}}-c_{\mathrm{org,i}}\right)-1+\sqrt{4m_0c_{\mathrm{org,i}}D^2+1}\right]\left(-1-\sqrt{4m_0c_{\mathrm{org,i}}D^2+1}\right)}\right|\right\}}{\pi r^2L\sqrt{4m_0c_{\mathrm{org,i}}D^2+1}} \quad (9)$$

3 Result and discussion

3.1 Flow pattern

3.1.1 Typical flow pattern

Figure 2 shows three distinct typical flow patterns in the RMCR.

$$\alpha=\frac{Q_{\mathrm{aq}}}{Q_{\mathrm{aq}}+Q_{\mathrm{org}}} \quad (10)$$

Where α is the phase fraction between water and kerosene. Figure 2(a) illustrates the formation process of slug flow (22), wherein the water and kerosene phases come into contact at the RMCR intersection and proceed together, eventually separating into two distinct liquid phases due to shearing motion. It is noteworthy that in slug flow, both the water and kerosene phases come into contact with the RMCR wall surface. In the same axial direction, the inner space of RMCR is occupied by a single-phase state. Slug breakage can be considered a result of the extrusion of the kerosene and water phases into the RMCR. The slug flow remains stable due to low flow rates and weak inter-fluid shear.

Figure 2(b) shows the development of parallel-droplet flow. The water and kerosene phases flow in parallel in the channel front section before the kerosene phase breaks evenly into small droplets, which continue flowing with water as the continuous

phase and kerosene as the dispersed phase. The droplet fracturing behavior exhibits fluctuations, with stability increasing as the phase fraction α increases. This fracturing occurs when the shear force between the phases surpasses the interfacial tension, causing the liquid at the kerosene phase front to separate (22).

Figure 2(c) demonstrates parallel flow (21). Following stable development, parallel flow maintains a form where water and kerosene phases exist in parallel within the channel, with no fluctuations at the phase interface. This flow pattern is prevalent when the total volumetric flow increases to a certain extent. In parallel flow, inertia force greatly exceeds interfacial tension, allowing the two-phase fluids to remain stable without fracturing. By increasing the total volumetric flow under any conditions, a stable parallel flow can ultimately be achieved.

Furthermore, carbon dust was used as a flow tracer to observe the internal flow of fluids and visualize the differences between the three typical flow patterns. Carbon dust was added to the kerosene at a ratio of 0.16 g per 100 g and left to stand for 5 minutes to form a stable suspension.

Figure 3 shows the internal flow of various flow patterns. Supporting Information (a-c) contains the original videos of Figure 3, which provide a better understanding of the flow. In general, the internal flow of kerosene varies under different flow patterns. In Figure 3(a), the movement track of toner in slug flow reveals that the flow speed at the center of the RMCR is notably higher than at other positions. Consequently, the carbon dust particles, initially at the tail, travel along the centerline to the kerosene

For Review Only

phase head and are pushed sideways. In Figure 3(b), a distinct velocity layer is observed in the kerosene phase during parallel flow. Within the kerosene phase, carbon dust particles near the phase interface progressively move ahead of those near the wall. As a result, the fluid velocity near the center of the tube is higher than that near the wall. In Figure 3(c), a turbulent internal spin is noticeable at the head of the kerosene phase (initial droplet) during parallel-droplet flow. As the front section of the parallel-droplet flow exhibits parallel flow, a high flow rate also occurs near the phase interface. This high-velocity zone extends to the head of the kerosene phase (initial droplet), inducing the internal spin. However, as the droplet detaches from the kerosene phase, its rotation speed gradually diminishes and eventually ceases.

Figure 4 further examines the internal spin of parallel-droplet flow. The movement of the flow can be seen in the videos provided in Supporting Information (d, e). The tracer streamline was also analyzed. Since particles and kerosene can be considered homogeneous, it can be processed using MATLAB (PIVLab 2.61) to obtain the corresponding vtk file. By importing the file result into paraview software, the flow field can be drawn. Figure 4(a) shows the spin in the head of the kerosene phase (initial droplet). The curved streamline of the initial droplet in Figure 4(a) effectively indicates that the internal fluid tends to rotate. The high-speed flow layer develops from the parallel-droplet flow front section, encircling the center within the head of the kerosene phase (initial droplet). The kinetic energy of the high-speed flow layer causes the head of the kerosene phase (initial droplet) to fully mix internally and be consumed by

For Review Only

friction between phase interfaces. Figure 4(b) shows the internal flow of the droplet in parallel-droplet flow. In contrast, the droplet streamline in Figure 4(b) is not curved, suggesting that the internal fluid is relatively static. The relative positions of carbon dust particles in the droplet remain constant over time, indicating that there is virtually no internal flow within the droplet. The droplet advances with the water phase. The similarities and differences in internal rotation between the two-phase fluids highlight the significant impact of shear force on the flow.

3.1.2 Effect of rotational speed on flow pattern

Figure 5 shows the flow patterns at various rotational speeds. When maintaining a constant total flow rate, the flow pattern transitions from slug flow to parallel-droplet flow as rotational speed increases, finally resulting in parallel flow. It becomes evident that the external centrifugal effect can indeed affect the flow pattern under identical conditions. This phenomenon could be attributed to the growing intensity of the external centrifugal force field, which causes a shift in the equilibrium among centrifugal effect, interfacial tension, and inertia force. As a result, the flow pattern changes at different rotational speeds.

3.1.3 Flow pattern transition

Figure 6 shows the transition curves of liquid-liquid flow patterns for the RMCR under various operational conditions. It is evident that the distribution of the three types of liquid-liquid flow patterns exhibits similar trends in different comparisons. The blue line signifies the boundary between slug flow and parallel-droplet flow, while the red

line demarcates the boundary between parallel-droplet flow and parallel flow. Slug flow primarily occurs in low total volumetric flow conditions and is less affected by rotational speed. As α increases, the sensitivity of the blue line to rotational speed progressively decreases. Parallel-droplet flow predominantly exists at medium total volumetric flow and is sensitive to rotational speed. With increasing α, the sensitivity of the red line to rotational speed continues to rise and becomes more pronounced than the blue line. Ultimately, when the total volumetric flow and rotational speed increase, the flow pattern transitions into parallel flow. It is worth noting that at high total volumetric flow, low rotational speed can result in parallel flow. However, under experimental conditions, increasing the rotational speed at low volumetric flow cannot produce parallel flow. Combined with the content in section 3.1.3, it can be concluded that the total volumetric flow is the decisive factor for the flow pattern, and the external centrifugal force field can expedite the transformation process.

Figure 6 only shows the direct effect of operating conditions on the flow pattern. If the effects of inertial forces, viscous forces, interfacial tension, and centrifugal effect on the flow pattern are considered, the operating conditions can be redescribed in dimensionless quantities to create a flow pattern distribution map. The relationship of parameter including volumetric flow of water (Q_{aq}), volumetric flow of kerosene (Q_{org}), liquid density (ρ), liquid viscosity (μ), interfacial tension between water and kerosene (σ), RMCR diameter (d), distance between the center of rotation and RMCR (r), angular velocity (ω) can be express as:

For Review Only

$$F(Q_{aq}, Q_{org}, \rho, \mu, \omega) = 0 \quad (11)$$

Based on the dimensional analysis, dimensionless groups were obtained as:

$$Re = \frac{\rho d u}{\mu} \quad (12)$$

$$\rho = \left(\frac{\alpha}{\rho_{water}} + \frac{1-\alpha}{\rho_{kerosene}} \right)^{-1} \quad (13)$$

$$\mu = \left(\frac{\alpha}{\mu_{water}} + \frac{1-\alpha}{\mu_{kerosene}} \right)^{-1} \quad (14)$$

$$Ca = \frac{\mu u}{\sigma} \quad (15)$$

$$\beta = \frac{\omega^2 r}{g} \quad (16)$$

where Re is Reynolds number, ρ is the mixing density, μ is the mixing viscosity, Ca is the Capillary number, β is the High gravity factor. The transition criterion from slug flow to parallel-droplet flow can be expressed as:

$$Ca^{-0.080}\alpha^{-0.087} = 2.39 Re^{-0.078}\beta^{0.002} \quad R^2 = 0.99 \quad (17)$$

The range of the parameters in Eq (16) are as follow: $53.01 < Re < 371.06$, $1.77 \times 10^{-3} < Ca < 1.24 \times 10^{-1}$, $0 < \beta < 4.47$ and $\alpha = 0.5/0.75/0.8$. Figure 7 illustrates the corresponding transition lines. Figure 7(a) shows that the area below the transition curve indicates the formation of the parallel-droplet flow and the area above the transition curve indicates the formation of the slug flow.

The transition criterion from parallel-droplet flow to parallel flow can be expressed as:

$$Ca^{-0.087}\alpha^{-0.094} = 2.55 Re^{-0.083}\beta^{0.014} \quad R^2 = 0.98 \quad (18)$$

For Review Only

The range of the parameters in Eq (17) are as follow: $53.01 < Re < 371.06$, $1.77\times10^{-3} < Ca < 1.24\times10^{-1}$, $0 < \beta < 4.47$ and $\alpha = 0.5/0.75/0.8$. Figure 7(b) illustrates the corresponding transition lines. Figure 7(b) shows that the area below the transition curve indicates the formation of the parallel flow and the area above the transition curve indicates the formation of the parallel-droplet flow.

Combined with the results presented by the operating conditions and dimensionless quantity, it is not difficult to find that Q_{total} and N have significant influence on the flow patterns in RMCR under liquid-liquid system. Furthermore, α, Re and β play a decisive role in the flow pattern.

3.2 Mass transfer

3.2.1 Effect of flow pattern on mass transfer performance

Figure 8 shows flow patterns and K_Oa under different conditions when $\alpha = 0.5$. The different flow patterns are distinguished by its color, and the influence of different flow patterns on the K_Oa can be seen. It can be seen that in Figure 8, for a given volumetric flow, an increase in rotational speed also results in an increase in K_Oa. The range of rotational speed covered in the experiment aligns with the range of rotational speed influencing flow patterns discussed in part 3.1.3. Moreover, the K_Oa increases with the increase of total volumetric flow. It becomes evident that the addition of rotational speed and the change of total volumetric flow can change the mass transfer performance of RMCR. Taking into account the two main operating conditions-rotational speed and total volumetric flow-it can be generally stated that the K_Oa of the

For Review Only

parallel flow is higher than $K_O a$ of parallel-droplet flow than $K_O a$ of slug flow. Reason of the difference in $K_O a$ may lie in the influence of flow pattern. According to the influence of rotational speed on the mass transfer performance and the flow pattern, it is speculated that the external centrifugal force field changes the flow pattern, and then changes its mass transfer characteristics.

3.2.2 Correlation of mass transfer coefficient

The empirical formula of $K_O a$ is further fitted as follow:

$$K_O a = 0.01 Re^{0.02} Ca^{0.05} \beta^{0.15} \left(\frac{u}{L}\right) \quad R^2 = 0.96 \tag{19}$$

Thus, we can use dimensionless quantity to predict $K_O a$. The range of the parameters in eq (17) are as follow: 0.067 mL/s < Q_{aq} < 0.470 mL/s, 0.067 mL/s < Q_{org} < 0.470 mL/s and 0 < β < 4.47. It can be observed that *Re*, representing the ratio of inertial force to viscous force, has relatively large exponents, resulting in a positive effect on $K_O a$, consistent with experimental data. *Ca*, expressing the ratio of viscous force to interfacial tension, also exerts a positive influence on mass transfer. Similarly, β, the ratio of centrifugal force to inertial force, positively affects mass transfer. This suggests that the external centrifugal force field indeed enhances the liquid-liquid heterogeneous mass transfer performance of the RMCR. The fitted correlation predicts all $K_O a$ values to be within ± 20% of the experimental data, as demonstrated in Figure 9.

4 Conclusions

For Review Only

In this study, a novel RMCR was proposed, and its liquid-liquid heterogeneous mass transfer performance was investigated in the water-benzoic acid-kerosene system using high-speed photography. Employing high-speed photography technology, we identified three typical flow patterns in the RMCR: slug flow, parallel-droplet flow, and parallel flow. Dimensionless fitting allows to determine the flow pattern transition criteria from slug flow to parallel-droplet flow and from parallel-droplet flow to parallel flow. Additionally, it is found that the total flow rate and rotational speed are the primary parameters governing the flow pattern. As the rotational speed and total flow rate increase, the $K_O a$ of the RMCR continues to rise, ranging from 0.003 to 0.021 s^{-1}. A correlation for predicting the mass transfer coefficient was proposed, and the predicted values showed good agreement with experimental values, with deviations within ±20%.

For Review Only

Acknowledgment

This work was supported by the National Natural Science Foundation of China (Nos. 22288102 and 22378011).

Supplementary materials

Figure S1. Standard curve of gas chromatography.

Supplementary data associated with this article can be found in the online version.

a. Behavior of the tracer in the slug flow - Figure 3(a) - 10 times speed down

b. Behavior of the tracer in the parallel-droplet flow - Figure 3(b) - 10 times speed

down

c. Behavior of the tracer in the parallel flow - Figure 3(c) - 100 times speed down

d. Behavior of the tracer in the parallel-droplet flow (initial droplet) - Figure 4(a) - 30 times speed down

e. Behavior of the tracer in the parallel-droplet flow (final droplet) - Figure 4(b) - 30 times speed down

For Review Only

Nomenclature

Q_{total}	total volumetric flow rate	mL/s
N	RMCR rotation speed	r/min
d	inner diameter of the RMCR	m
N_O	mole flux of benzoic acid	mol/(m^2·s^1)
D	ratio of kerosene phase to water phase	-
V_{RMCR}	The volume of the RMCR	m^3
a	specific surface area	m^2/m^3
K_O	overall mass transfer coefficient	m/s
$C_{aq,i}$	concentration of benzoic acid in the water phase at the inlet	mol/m^3
$C_{aq,o}$	concentration of benzoic acid in the water phase at the outlet	mol/m^3
$C_{org,i}$	concentration of benzoic acid in the kerosene phase at the inlet	mol/m^3
$C_{org,o}$	concentration of benzoic acid in the kerosene phase at the outlet	mol/m^3
C^*_{org}	concentration of benzoic acid in the kerosene phase at equilibrium	mol/m^3
V_{RMCR}	volume within the RMCR	m^3
L	length of the RMCR	m
r	The radius of rotation of RMCR	m

Greek Letters

ρ	density	kg/m^3
μ	viscosity	mPa·s
σ	interfacial tension between water and kerosene	mN/m
ω	RMCR angular velocity	rad/s
β	high gravity factor	-

For Review Only

α	phase fraction between water and kerosene	-

Dimensionless group

Re	Reynolds number
Ca	Capillary number

Abbreviations

RMCR	Rotating millimeter channel reactor
MCR	Millimeter channel reactor

For Review Only

References

1.Wang K, Luo GS. Microflow extraction: A review of recent development. Chemical Engineering Science. 2017;169:18-33.

2.Mills PL, Quiram DJ, Ryley JF. Microreactor technology and process miniaturization for catalytic reactions - A perspective on recent developments and emerging technologies. Chemical Engineering Science. 2007;62(24):6992-7010.

3.Doku GN, Verboom W, Reinhoudt DN, van den Berg A. On-microchip multiphase chemistry - A review of microreactor design principles and reagent contacting modes. Tetrahedron. 2005;61(11):2733-2742.

4.Mae K. Advanced chemical processing using microspace. Chemical Engineering Science. 2007;62(18-20):4842-4851.

5.Assmann N, Ładosz A, Rudolf von Rohr P. Continuous Micro Liquid-Liquid Extraction. Chemical Engineering & Technology. 2013;36(6):921-936.

6.Porta R, Benaglia M, Puglisi A. Flow Chemistry: Recent Developments in the Synthesis of Pharmaceutical Products. Organic Process Research & Development. 2015;20(1):2-25.

7.Sattari-Najafabadi M, Nasr Esfahany M, Wu Z, Sunden B. Mass transfer between phases in microchannels: A review. Chemical Engineering and Processing - Process Intensification. 2018;127:213-237.

8.Yao CQ, Zhao YC, Chen GW. Multiphase processes with ionic liquids in microreactors: hydrodynamics, mass transfer and applications. Chemical Engineering

For Review Only

Science. 2018;189:340-359.

9.Angeli P, Tsaoulidis D, Hashi Weheliye W. Studies on mass transfer of europium(III) in micro-channels using a micro Laser Induced Fluorescence technique. Chemical Engineering Journal. 2019;372:1154-1163.

10.Tan J, Xu JH, Li SW, Luo GS. Drop dispenser in a cross-junction microfluidic device: Scaling and mechanism of break-up. Chemical Engineering Journal. 2008;136(2-3):306-311.

11.Roques-Carmes T, Monnier H, Portha JF, Marchal P, Falk L. Influence of the plate-type continuous micro-separator dimensions on the efficiency of demulsification of oil-in-water emulsion. Chemical Engineering Research and Design. 2014;92(11):2758-69.

12.Kolehmainen E, Turunen I. Micro-scale liquid-liquid separation in a plate-type coalescer. Chemical Engineering and Processing: Process Intensification. 2007;46(9):834-839.

13.Xu JH, Tan J, Li SW, Luo GS. Enhancement of mass transfer performance of liquid-liquid system by droplet flow in microchannels. Chemical Engineering Journal. 2008;141(1-3):242-249.

14.Hossain S, Lee I, Kim SM, Kim KY. A micromixer with two-layer serpentine crossing channels having excellent mixing performance at low Reynolds numbers. Chemical Engineering Journal. 2017;327:268-277.

15.Shao H, LÜ Y, Wang K, Luo GS. An Experimental Study of Liquid-Liquid Microflow Pattern Maps Accompanied with Mass Transfer. Chinese Journal of

For Review Only

Chemical Engineering. 2012;20(1):18-26.

16.Singh S, Kumar UKA. Hydrodynamics and Mass Transfer Studies of Liquid-Liquid Two-Phase Flow in Parallel Microchannels. International Journal of Multiphase Flow. 2022;157:104248.

17.Cao Y, Li J, Jin Y, Luo JH, Wang YB. Liquid-liquid two-phase mass transfer characteristics in a rotating helical microchannel. Chinese Journal of Chemical Engineering. 2019;27(12):2937-2947.

18.Fan CX, Guo ZN, Luo JH. Study on an improved rotating microchannel separator in the intensification for demulsification and separation process. Chinese Journal of Chemical Engineering. 2022;55:181-191.

19.Gandharv S, Kaushik P. Transient electro-osmotic flow in rotating soft microchannel. Physics of Fluids. 2022;34(8):082023.

20.Bai S, Li WS, Liu W, Luo Y, Chu GW, Chen JF. Micromixing efficiency intensification of a millimeter channel reactor in the high gravity field. Chemical Engineering Science. 2022;251:117407.

21.Li WP, Xia FS, Zhao SC, Zhang MQ, Li W, Zhang JL. Characterization of liquid-liquid mass transfer performance in a novel pore‐array intensified tube‐in‐tube microchannel. AIChE Journal. 2019;66(4).

22 Shin, H.C.; Kim, S.M. Experimental investigation of two-phase flow regimes in rectangular micro-channel with two mixer types. Chemical Engineering Journal 2022, 448:137581.

For Review Only

418

419

For Review Only

Figure Captions

Figure 1. Schematic diagram of (a) experimental setup and (b) RMCR.

Figure 2. Typical dynamic process of (a) image acquisition window, (b) slug flow when Q_{total} = 0.134 mL/s and α = 0.5, (c) parallel-droplet flow when Q_{total} = 0.281 mL/s and α = 0.8, (d) parallel flow when Q_{total} = 1.54 mL/s and α = 0.5.

Figure 3. Behavior of the tracer in the (a) slug flow, (b) parallel-droplet flow, (c) parallel flow.

Figure 4. Streamline of internal rotation flow of parallel-droplet flow in different stages (a) initial droplet, (b) droplet.

Figure 5. Effect of rotational speed on flow pattern when (a) Q_{total} = 0.267 mL/s and α = 0.5, (b) Q_{total} = 0.134 mL/s and α = 0.75, (c) Q_{total} = 0.134 mL/s and α = 0.8.

Figure 6. Liquid flow pattern transition curves for (a) α = 0.5, (b) α = 0.75, (c) α = 0.8.

Figure 7. Liquid flow transition criteria from (a) slug flow to parallel-droplet flow, (b) parallel-droplet flow to parallel flow.

Figure 8. Flow patterns and $K_O a$ under different operating conditions.

Figure 9. Comparison of predicted and experimental values of $K_O a$.

Table Legend

Table 1. Physical properties of mass transfer system (20 ℃).

For Review Only

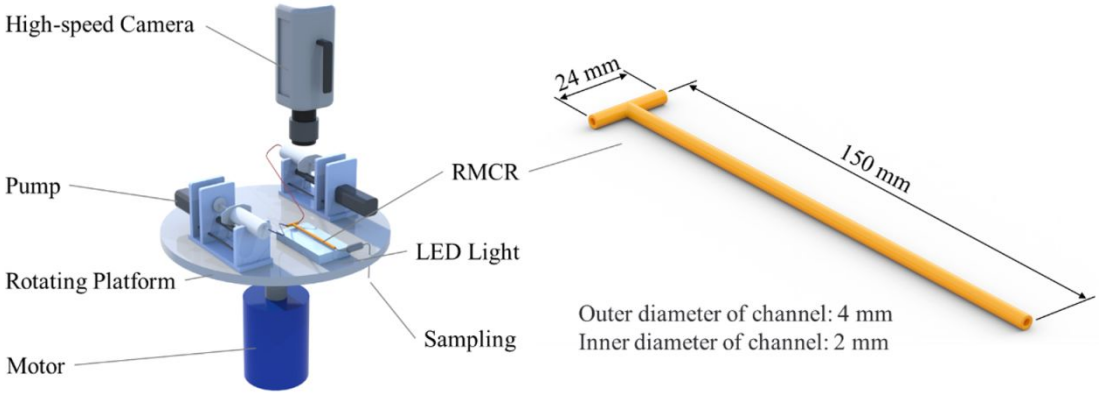

(a) (b)

Figure 1. Schematic diagram of (a) experimental setup and (b) RMCR.

For Review Only

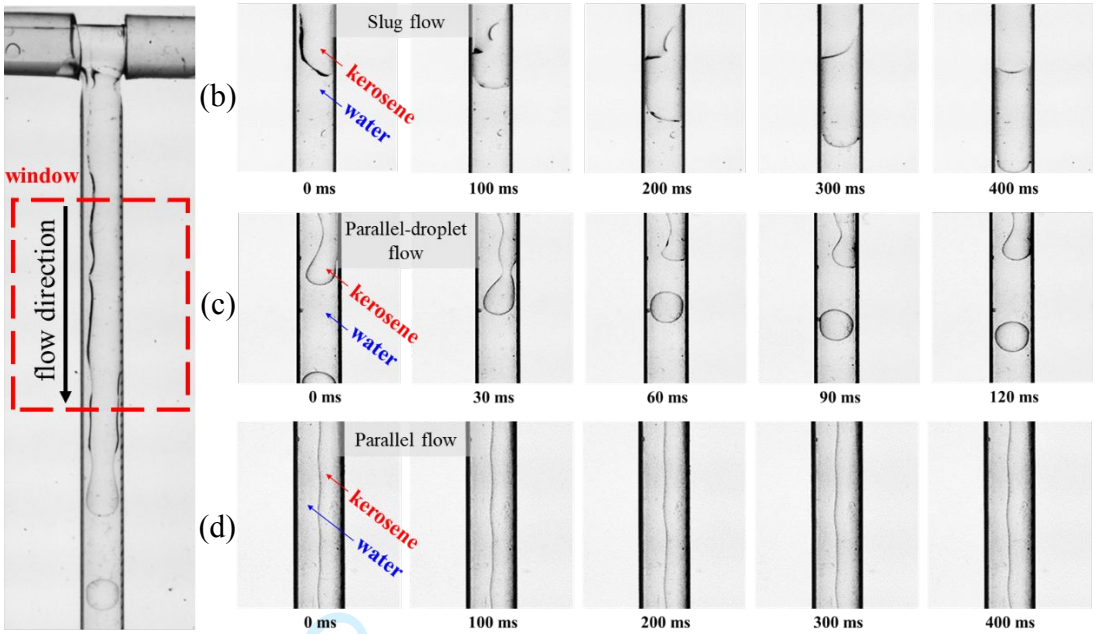

Figure 2. Typical dynamic process of (a) image acquisition window, (b) slug flow when Q_{total} = 0.134 mL/s and α = 0.5, (c) parallel-droplet flow when Q_{total} = 0.281 mL/s and α = 0.8, (d) parallel flow when Q_{total} = 1.54 mL/s and α = 0.5.

For Review Only

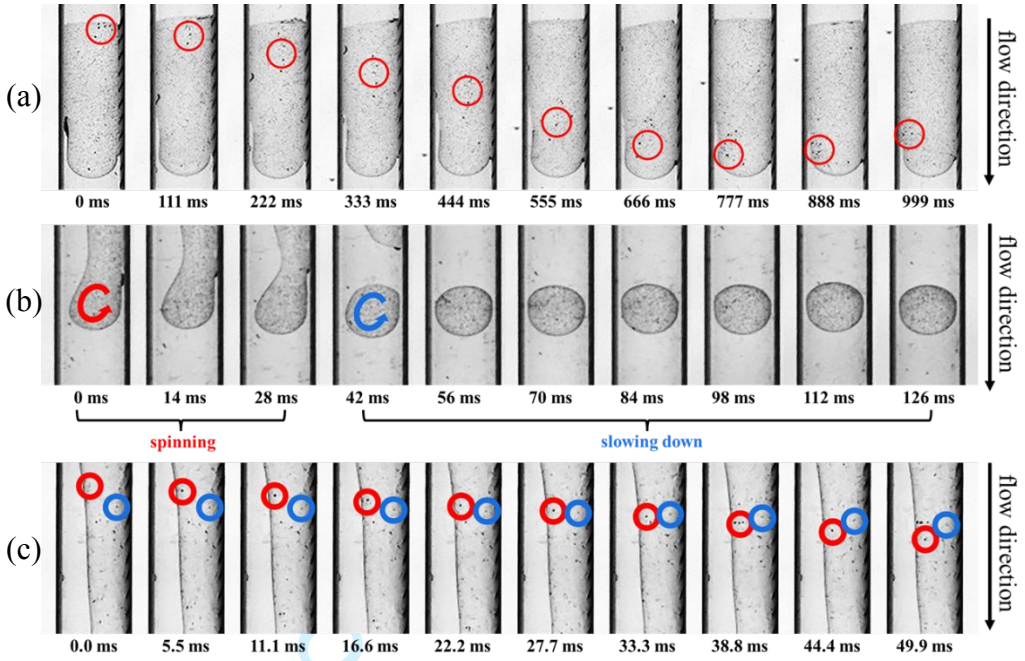

Figure 3. Behavior of the tracer in the (a) slug flow, (b) parallel-droplet flow, (c) parallel flow.

For Review Only

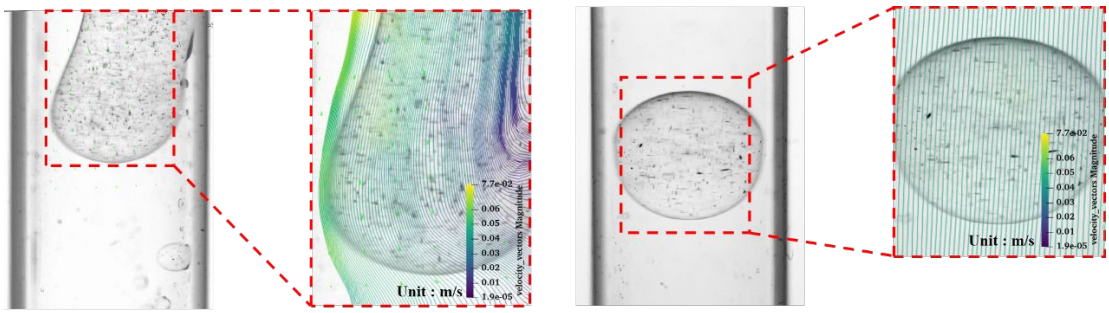

(a) (b)

Figure 4. Streamline of internal rotation flow of parallel-droplet flow in different stages (a) initial droplet, (b) droplet.

For Review Only

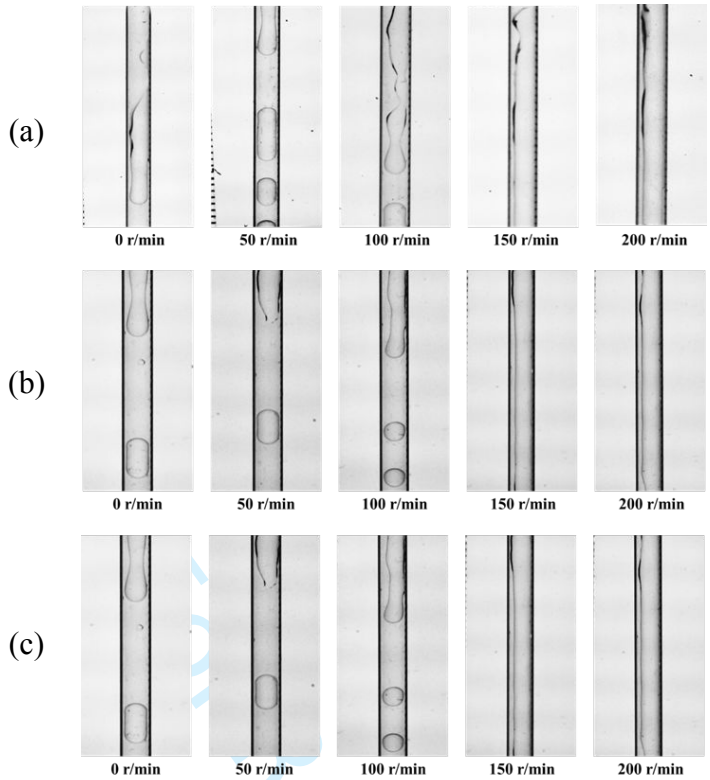

Figure 5. Effect of rotational speed on flow pattern when (a) Q_{total} = 0.267 mL/s and α = 0.5, (b) Q_{total} = 0.134 mL/s and α = 0.75, (c) Q_{total} = 0.134 mL/s and α = 0.8.

For Review Only

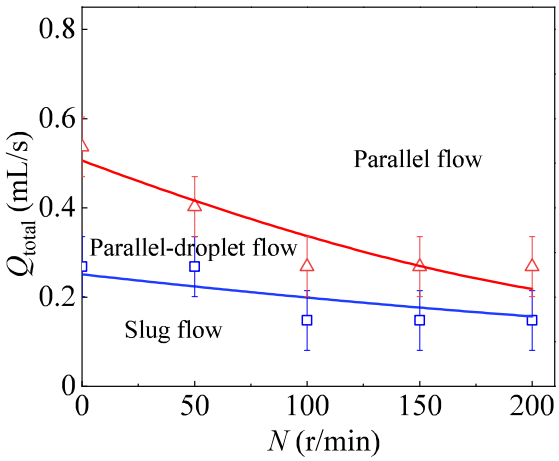

(a)

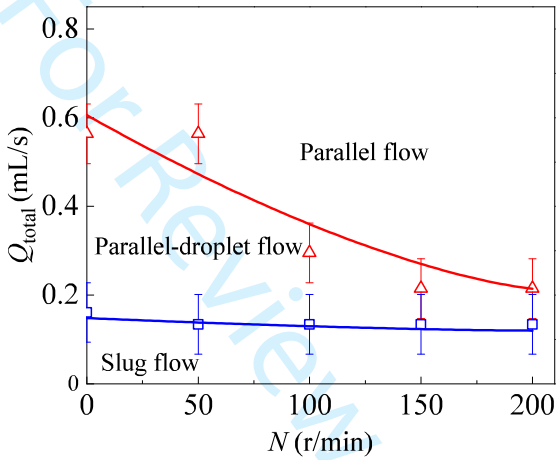

(b)

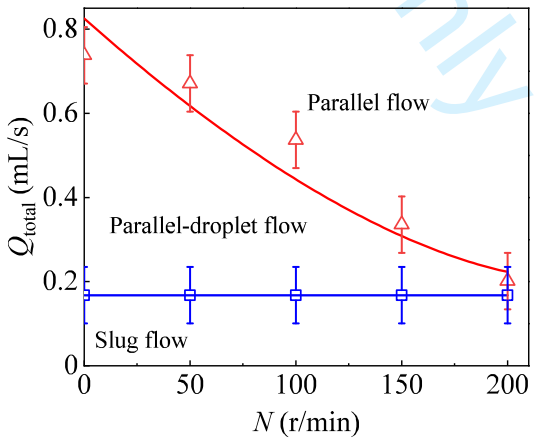

(c)

Figure 6. Liquid flow pattern transition curves for (a) $\alpha = 0.5$, (b) $\alpha = 0.75$, (c) $\alpha = 0.8$.

For Review Only

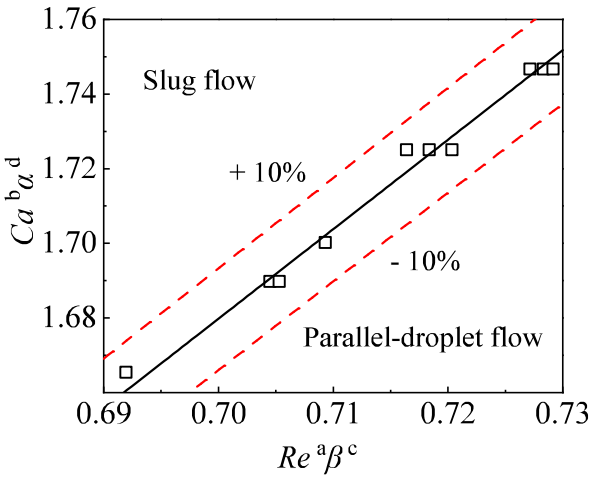

(a)

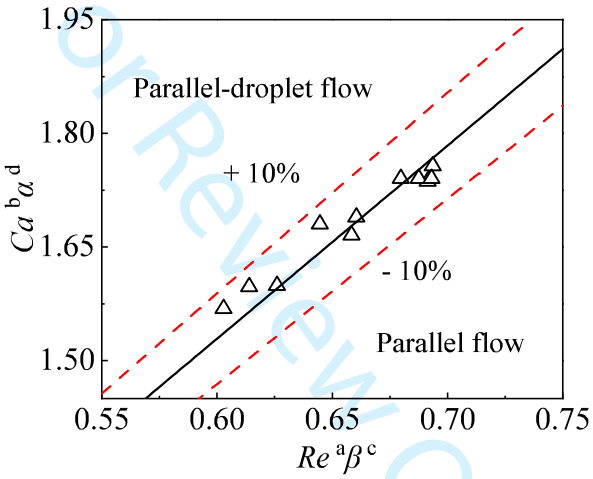

(b)

Figure 7. Liquid flow transition criteria from (a) slug flow to parallel-droplet flow, (b) parallel-droplet flow to parallel flow.

For Review Only

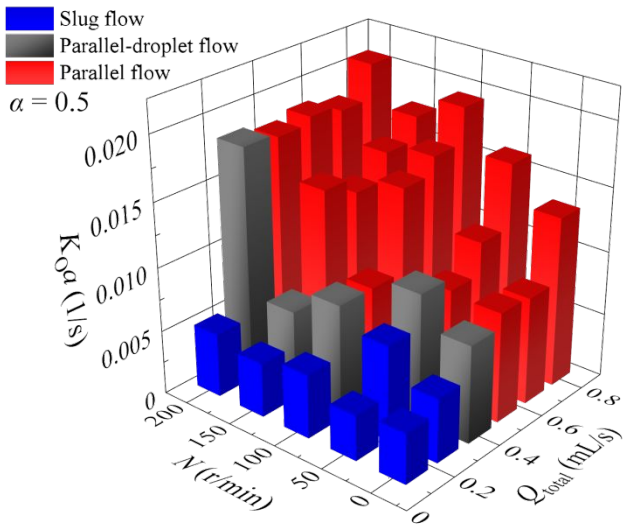

Figure 8. Flow patterns and K_Oa under different operating conditions.

For Review Only

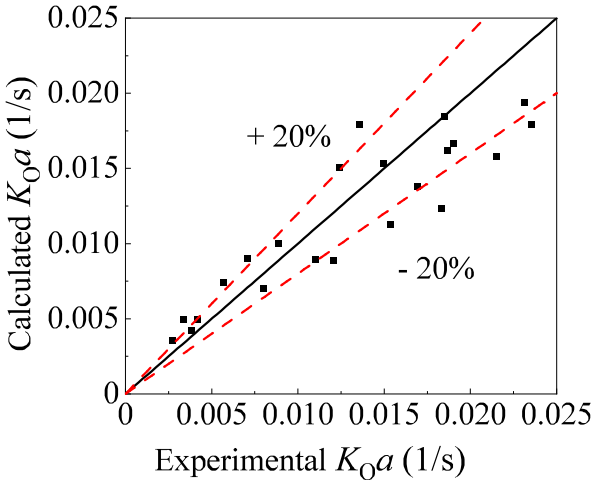

Figure 9. Comparison between predicted and experimental values of $K_O a$.

For Review Only

Table 1. Physical properties of mass transfer system (20 ℃)

Phase	Solvend	ρ / kg·m^{-3}	μ / mPa·s	σ / mN·m^{-1}
Water	-	998.182	1.005	34.574
Kerosene	benzoic acid (0.2w%)	799.096	2.500	

For Review Only